Unterschrift des Betreuers

TU WIEN
TECHNISCHE UNIVERSITÄT WIEN

D I P L O M A R B E I T

Engineering of protein purification from *Escherichia coli* homogenates

Thema

Ausgeführt am

Department für Biotechnologie, Universität für Bodenkultur, Wien

Assoc. Prof. Dipl.-Ing. Dr. Rainer Hahn (BOKU) und
unter der Anleitung von   Privatdoz. Mag.rer.nat. Dr. Bernhard Seiboth (TU Wien)

durch

Ing. Bernhard Sissolak, B.Sc.

Name

Reifgasse 13/1/2; A-3500 Krems an der Donau

Anschrift

_____   _____
Datum   Unterschrift (Student)

Ing. Bernhard Sissolak, BSc.

Engineering of protein purification from Escherichia coli homogenates

Master's Thesis

Technical University of Vienna

Institute of Chemical Engineering
Head: Univ.Prof. Dipl.-Ing. Dr.techn. Anton Friedl

Supervisor: Assoc. Prof. Dipl.-Ing. Dr. Rainer Hahn & Privatdoz. Mag.rer.nat. Dr. Bernhard Seiboth

Vienna, July 2015

Statutory Declaration

I declare that I have authored this thesis independently, that I have not used other than the declared sources/resources, and that I have explicitly marked all material which has been quoted either literally or by content from the used sources.

Vienna, _____   _____

        Date   Signature

Eidesstattliche Erklärung[1]

Ich erkläre an Eides statt, dass ich die vorliegende Arbeit selbstständig verfasst, andere als die angegebenen Quellen/Hilfsmittel nicht benutzt, und die den benutzten Quellen wörtlich und inhaltlich entnommenen Stellen als solche kenntlich gemacht habe.

Wien, am _____   _____

        Datum   Unterschrift

---

[1]Beschluss der Curricula-Kommission für Bachelor-, Master- und Diplomstudien vom 10.11.2008; Genehmigung des Senates am 1.12.2008

Danksagung

Es war eine große Ehre für mich in der PilotAnalge arbeiten zu dürfen. Die Errichtung dieser war nicht nur wichtig für mich sondern wird auch Generationen von Studenten die Möglichkeit bieten im Pilot Maßstab arbeiten zu dürfen. Der große Andrang bei der Übung "BioProcess Labratory" bestätigt dass hier etwas Großes geleistet worden ist. Es freut mich, dass sich hier Universitäten zusammengeschlossen und Geld in die Hand genommen haben um hier etwas Beeindruckendes zu schaffen. Solcherart von Kooperation sollten noch viel vermehrter stattfinden, denn eine Universität alleine hätte dies vermutlich nicht stemmen können.

Meine ganze Arbeit wäre nicht zustande gekommen hätten mir folgende Leute nicht dabei geholfen: Die PilotPlant Crew ist mir sehr ans Herz gewachsen und werde ich auch nie mehr vergessen. Technikums Leiter Markus Luchner und Techniker Clemens Kainprecht haben mir sehr geholfen und standen mir immer beiseite. Ohne euch würde der Betrieb nicht laufen. Vielen Dank.

Außerdem möchte ich noch ausdrücklich Sabine Necina danken, die mir immer mit Rat und Tat beiseite stand. Du hast mir sehr viel Arbeit abgenommen. Auch dir ein großes Dankeschön.

Nun zu meinen lieben Betreuern. Bernhard ich danke dir für deine Geduld die du mir aufgebracht hast. Und das du mir die Möglichkeit gegeben hast außerhalb der TU Wien meine Diplomarbeit zu machen. Lieber Rainer, ich danke dir von großen Herzen, dass du mir dein Vertrauen geschenkt hast und mich bei dir aufgenommen hast. Ich habe sehr viel gelernt bei dir. Vor allem meine Selbstorganisation und Arbeitsweise hat sich durch dich, zum positiven, geändert.

Natürlich möchte ich auch all meinen Kollegen von Department für Biotechnologie bedanken die mich begleitet haben. Viele neue Freunde habe ich hier gewonnen und alle haben ein Stück dazu beigetragen dieses Werk hier zu vollenden. Danke Moritz das du die Zeit aufgewendet hast um mir Python bei gebracht zu haben.

Danke auch an meine Familie, meine Eltern die mir das Studium ermöglicht haben. Danke für all die Unterstützung sowohl im- als auch materiell. Ohne euch wäre ich nicht hier.

Liebe Kerstin, danke dass du mir die ganze Zeit über zur Seite stehst. Ich Liebe dich.

Abstract

The term Quality by Design defines a concept for processing biologics in pharmaceutical biotechnology. In short it means that quality is built into the product rather than prove it afterwards. Knowing the product and even more a fully understanding of the process is mandatory. This work helps to gain process knowledgment of industrial downstream processing of *E.coli* homogenates.

Escherichsa coli (*E. coli*) is a well-known microorganism, easy to manipulate and popular in biotechnology processes. The fermentation process is fast, cheap and simple. Due to the lack of secretion properties isolation and purification of recombinant proteins is challenging.

To characterize the unit operations and their mutual influence, the *E. coli* strain HMS 174 (DE3) with the plasmid pET11a-GFPmut3.1 was used to establish a downstream model process. GFP was chosen because of its easy quantification. The recently established *BIO INDUSTRIAL PILOT PLANT* provided the possibility to work on a pilot scale level.

First part of the investigation was the homogenization and its effectiveness in dependence of cell density, number of passages and operating pressure. Over the whole range of operating pressure (20 MPa to 90 MPa) cell density had a negligible effect on the breakage of the cells. Above 60 MPa over 90% protein release was achieved with one passage. The disruption efficiency was highly dependent on operating pressure.

It was also possibly to establish a correlation between solid content in the solution and its viscosity. It provides a useful estimate of solid content with a short measurement. This is particularly useful for design of centrifuge separations.

Furthermore, the influence of the homogenization on the centrifugation behavior was studied. It could be shown that, the higher the operating pressure and the more passages had been performed the clearance efficiency was dramatically decreasing.

Another important point is the reduction factor of the pellet volume. At high cell density the pellet volume reduction was lower, leading to more discharges when the homogenate was clarified in a disc stack centrifuge. In turn, this led to significant product losses because 0.4 L of liquid is discharged during every ejection.

The chromatographic capture step using anion exchange chromatography was investigated with the resins CaptoQ and Q-Sepharose FF in detail for crude and diafiltrated homogenate. Adsorption isotherms revealed a displacement effect of GFP by other components at high feed concentrations. The displacement can be modeled by the extended Langmuir isotherm, which takes into account the variable θ_i. It represents the available binding sites for each component and it is suggested to be in correlation with their molecular size. Additionally, was investigated the adsorption kinetics of the diafiltrated and crude homogenate. Kinetic measurements showed that an overshoot above equilibrium capacity took place. The higher the feed concentration the more pronounced was the overshoot. According to these data, it is suggested that a low residence time and a high feed concentration is required to obtain the maximum binding capacity. In general, CaptoQ had a higher binding capacity than Q-Sepharose FF. Also diafiltrating the homogenate enhanced binding capacity. Furthermore break through curves (BTC) were performed with both resins. Remarkably, changes in the residence time had no effect on the dynamic binding capacity (DBC) for the crude homogenate. Additionally, a higher DBC was exhibited at a higher feed concentration. However, the recovery in the elution step was quite low due to the fact that a high amount of product was lost during the wash out phase. BTC's with the diafiltrated revealed a higher binding capacity which was positively influenced by enhancing the residence time and lowering the feed concentration.

Contents

List of Figures

List of Figures

List of Tables

Abbreviations

θ_i ......Occupied binding sites by component i
Σ ......Cross sectional area of a gravity settler
ω ......angular velocity
BTC   ......Break through curve
CIP   ......Cleaning in place
CV   ......Column volume in mL
DBC   ......Dynamic binding capacity
DSP   ......Downstream processing
EBC   ......Equilibrium binding capacity
Fl   ......Factor for the non used filtration area
GFP   ......Green fluorescent protein
Gly   ......Glycin
HIC   ......Hydrophobic chromatography
IEX   ......Ion exchange chromatography
IPTG   ...... β D-1 thiogalactopyranosid
Ka   ......Adsorption constant in $\frac{mL}{mg}$
NTU   ......Nephelometric units
PBS   ......Phosphate buffer saline
pI   ......Isoelectric point
Q   ......Frowrate throughput of a centrifuge
q   ......Binding capacity in $\frac{mg_{GFP}}{mL_{resin}}$
R   ......Protein release
SEC   ......Size exclusion chromatography
Ser   ......Serin
Tyr   ......Tyrosin
$u_{g,c}$ ......Gravitational and centrifugal force
UV/DF   ......Ultra - / Diafiltration

1. Introduction

1.1. The Green Fluorescent Protein GFP

1.1.1. The discovery of GFP

In the 1960's, Osamu Shimomura's research was dealing with bioluminescence. This is the ability of organisms like bacteria, fungi but also of invertebrates and vertebrates to generate light by itself or to live in symbiosis with another organism. Light is generated through chemical reactions like oxidation of luciferin catalyzed by luciferase with a result of dissipating excess energy in form of light. Another opportunity is the use of photo proteins as it does happen e.g. in marine organism like in jellyfish.

Aequorea victoria (see figure 1.1), was the research object in the study of Shimomura et al. (1962). They isolated two proteins from this invertebrate, aequorin and a brightly fluorescencing one which was later named green fluorescent protein (GFP) by Morin and Hastings (1971). The scientific impact of GFP was and still is tremendous. Chalfie et al. (1994) established to express GFP in prokaryotic as well as eukaryotic cells, *Escherichia Coli* (*E. coli*) and *Caenorhabditis elegans* (*C. elegans*) respectively and managed to use it as a marker to track or rather localize proteins of interest in a living cell. Tsien (1998) improved the understanding of chromophore formation and produced new variants of GFP and GFP-like proteins with enhanced brightness. "For the discovery and development of the green fluorescent protein, GFP" Osamu

Figure 1.1.: The jellyfish *Aequorea victoria* (Sanders, Jeremy K M and Jackson, 2009)

Shimomura, Martin Chalfie and Roger Y. Tsien received the Nobel Prize in Chemistry 2008 (Sanders, Jeremy K M and Jackson, 2009). Until now, a lot of engineering work has been done to improve different characteristics of this protein. Therefore it became one of the most used and best known proteins in the scientific community.

1.1.2. Structure of GFP and folding characteristics

The *primary structure* of GFP reveals a 238 amino acids long peptide chain of around 26.9 kDA. In the native protein the chromophore, *p*-hydroxybenzylidenimidazoline (HBI), is spontaneously formed from the residues 65 - 67, Serine, Tyrosine and Glycine, respectively (Ser-Tyr-Gly). In figure 1.2 it is shown that the formation of the protein depends on various steps. At first, folding of the protein in its almost native conformation takes place which is relatively fast and leads to the folded but reduced and therefore non flourescenting intermediates. This state initiates the cyclization and dehydration process of the tripeptide motif followed by oxidation. The protein is not able to gain it's typically fluorescence characteristic, until this confirmation is obtained. Heim et al. (1994) proposed that the two absorbance bands at around 400 nm and 470 nm in the spectrum could be derived from the protonated and deprotonated species. Furthermore, they established to grow *E. coli* under anaerobically conditions. The so produced GFP was not fluorescent. This does imply that atmospheric oxygen is needed for establishing a functioning protein. Tsien (1998) claimed that refolding is relatively insensitive to GFP concentrations and added cofactors.

Reid and Flynn (1997) characterized the kinetics of formation of active GFP and showed that the limiting step of this process is the chromophore formation and not the protein folding itself. As shown in figure 1.3 it is apparent that the step from folded reduced non fluorescent to the oxidized flourescenting one is exceedingly slow, in comparison to the folding of the protein. This a crucial point in terms of refolding of insoluble aggregates from *E. coli*, so called inclusion bodies (IB).

The GFP wild-type possesses two excitation bands at about 400 nm and a slighter one at 470 nm. The emission spectrum has a maximum at 505 nm (see figure 1.4). Depending on its chromophore components e.g. wild-type is a mixture of neutral phenol and anionic phenolate, the excitation and emission spectra vary. Therefore the protein variants are divided into several classes according to its chromophore composition. The *tertiary structure* of GFP is an eleven-stranded β-barrel, in which an α-helix is running through. The chromophore is attached in the center of the α-helix. (Tsien, 1998)
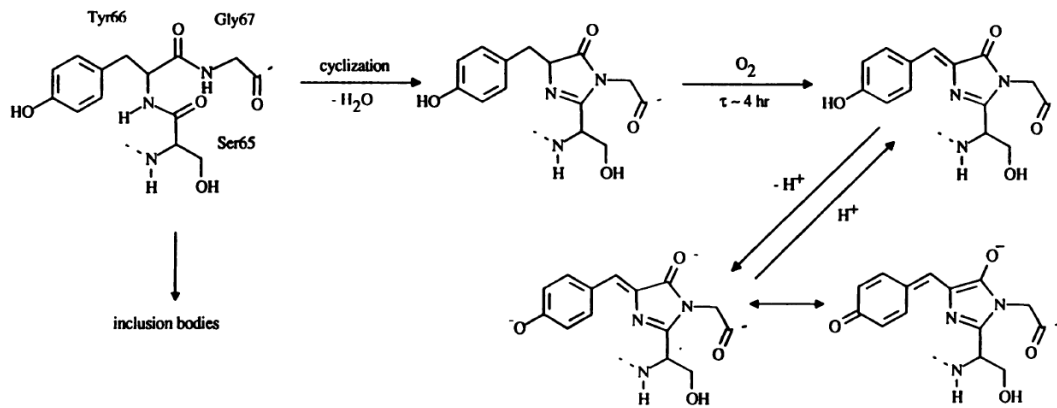
Figure 1.2.: Biosynthetic mechanism of chromophore formation as proposed by Heim et al. (1994)
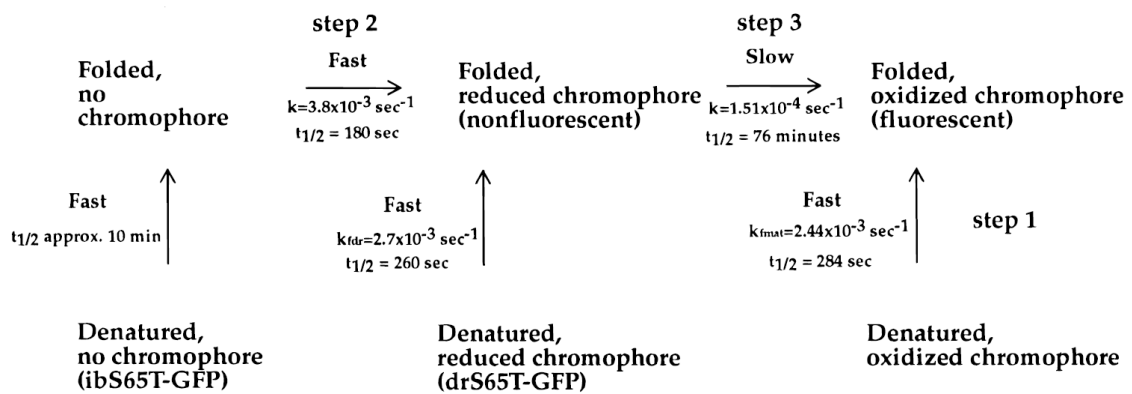
Figure 1.3.: Schematic pathway of chromophore formation as proposed by Reid and Flynn (1997)
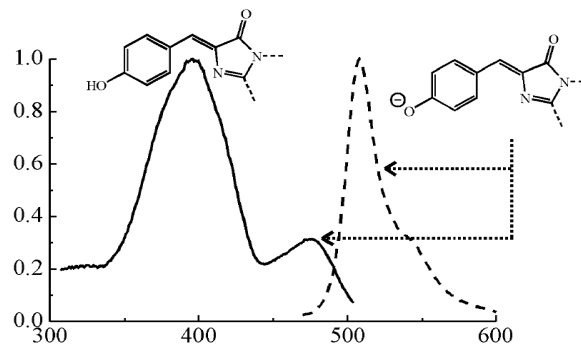
Figure 1.4.: Normalized emission (bold line) and fluorescence excitation spectra (dashed line) of GFP from the wild-type class. Also shown the chromophore which are assumed to be responsible for those absorbance bands (Left: protonated; Right: deprotonated). (Tsien, 1998)

1.2. The host cell Eschericha coli

Bacterial hosts are often used for the production of recombinant proteins. Approximately 30% of current biopharmaceuticals are produced by those cells. The running costs are low due to shorter process times and low expenses for culture media. *Escherichia coli* belongs to the phylum proteobacteria. It is a facultative anaerobic, rod shaped and gram-negative prokaryotic organism. It is well characterized, known and used for many years. Insulin was the first recombinant protein produced in *E. coli* which was approved by the US Food and Drug Administration. (Overton, 2014)

In figure 1.5 an outline of a recombinant protein production is shown. Usually, the desired gene is cloned into the multiple cloning sites which are controlled by a promoter. The vector gets transformed into *E. coli*. After a certain stage of growth the promoter gets activated by a chemical inducer.

For *E.coli* different promoters are available. According to Overton (2014) the commonly used promoters are:

- induced by IPTG
  - pET system (DE3/T7)
  - *lac* systems (*Plac, PlacUV5*)
  - *lac/trc*
- induced by arabinose
  - pBAD
- induced by temperature
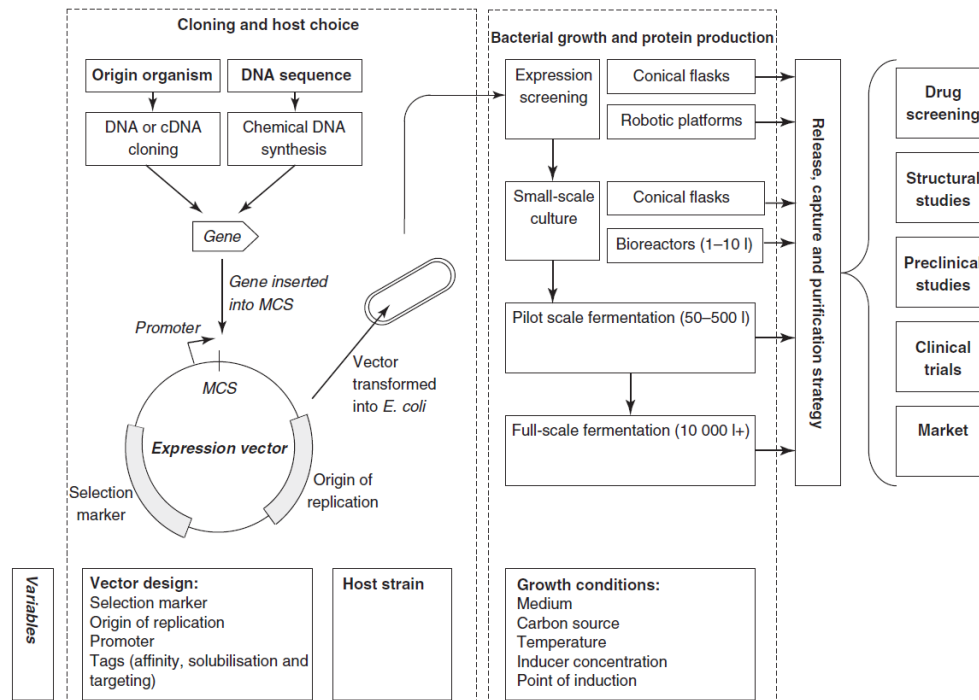
Figure 1.5.: Outline of a recombinant protein production in *E. coli*. (Overton, 2014)

- λ / p_l

The pET vector system (DE3/T7) is based on the activity of the T7 RNA polymerase (see figure 1.6). The T7 RNA polymerase gene is located in the genome of *E. coli* and is under control of the *lac* promoter. The *lac* repressor is bound on the promoter and inhibits him.

In the presence of β-D-1-thiogalactopyranoside (IPTG), an artificial inductor of the *lac*-operon, the transcription of the T7 RNA polymerase starts. The pET vector possesses a T7 promoter, which is also inhibited by the *lac* repressor, where only the T7 RNA polymerase can bind and activates the transcription of the gen of interest. The pET vector system is strong but leaky. Even though IPTG is not present, small amounts of T7 RNA polymerase are produced together with the protein of interest. This can lead to inclusion bodies formation and to a decrease in the growth rate of cells (i.e. when toxic proteins are going to be produced). (Overton, 2014; Novagen, 2003)

Normally, recombinant proteins are located in the cytoplasm. This has some disadvantages like high proteases activity and the reducing environment. Also the cells must be completely disrupted to release the protein. Translocation of the protein into the periplasmatic space or secretions of the protein into the media are potential options to improve the production process. *E. coli* usually use the secretory pathway
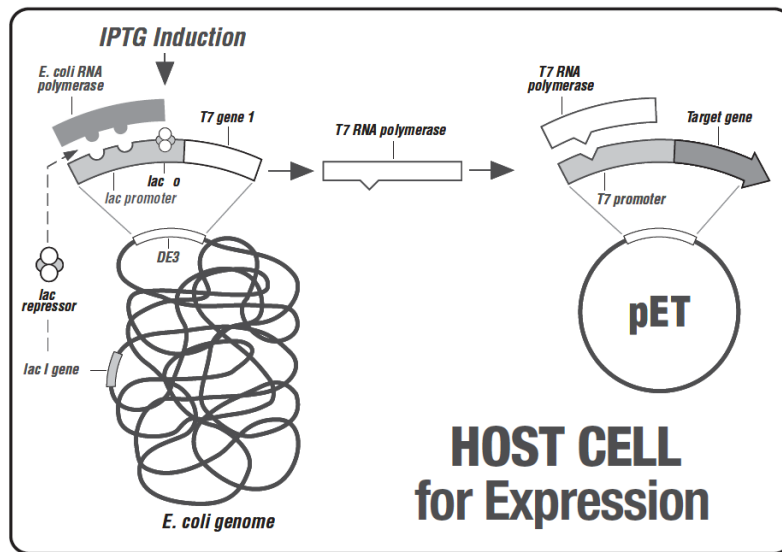
Figure 1.6.: Schematic mechanism of the pET system (DE3/T7) in *E. coli*. (Novagen, 2003)

to discharge high molecular weight toxins and exoenzymes. This is done in one step (type 1 secretion mechanism) or in a 2-step process with an intermediate in the periplasmatic space (type 2 secretion mechanism). (Mergulhão, F J M et al., 2005)

1.3. Overview of the purification process of recombinant GFP produced in E. coli

A flow chart of the purification process is shown in figure 1.7. At first, the cell broth is centrifuged to separate the cells from the culture medium. The solid content after this step should be as high as possible. This has the advantage of having a smaller volume which could be stored at 4°C for some days or rather be frozen at -20°C for long time storing. Then adjustment of the desired cell suspension with a specific buffer is required. In the next step homogenization is carried out to break up the cells, resulting in a release of the protein. Again centrifugation is used to separate the cell debris and any other non-soluble components like inclusion bodies. At this point there are two possible ways to proceed further on.

If the soluble protein is required the supernatant is cautiously decanted and filtrated through a 0.2 μm filter. Due a relatively high salt concentration in the homogenization buffer, which does affect the ion exchange chromatography (IEX) in the next step, a replacement by a non-salt buffer is needed. This is accomplished by diafiltration. If
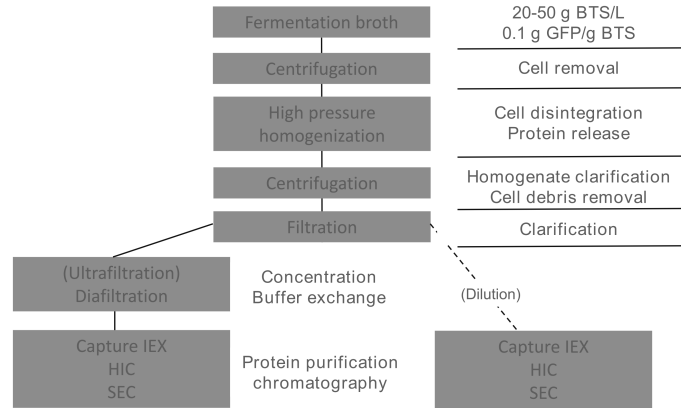
Figure 1.7.: General downstream process flow chart with its different unit operations

the solution possesses a high protein titer no extra ultrafiltration is required. After that, a three step chromatography process is carried out. At first, capturing of the protein is performed by anion exchange chromatography followed by an intermediate purification through a hydrophobic interactions chromatography (HIC) and polishing with a size exclusion chromatography (SEC).

1.4. Centrifugation characteristic and its underlying theory

Regardless of the expression type, intracellular or secreted, cell recovery or rather removal is essential. Centrifugation is used for separation of fluid/fluid or solid/fluid suspensions. The mechanism is based on the difference of density between the phases in an acceleration field which causes distinct particle movements. The velocity of a particle under gravitational force u_g is given by Stoke's Law (see equation 1.1), where ρ_L is the density of the solution, ρ_P density of the particle, μ the viscosity of the liquid, D_p the particle diameter and g the gravitational acceleration. Analogously the terminal velocity in a centrifugal force u_c is given by equation 1.2. Here, ω is the angular velocity and r the distance from the center of the centrifuge to the outer wall. (Doran, 2012)

1. Introduction

$$u_g = \frac{(\rho_p - \rho_L)}{18\mu} D_p^2 g \tag{1.1}$$

$$u_c = \frac{(\rho_p - \rho_L)}{18\mu} D_p^2 \omega^2 r \tag{1.2}$$

To compare the performance and for upscaling purposes of different centrifuges the parameter Σ is useful. It represents the cross sectional area of a gravity settler which is required to obtain the same separation efficiency as a corresponding centrifuge, assuming that particles are spherical and no sedimentation hindrance occurres (see equation 1.3). If the compared centrifuges differ, in a geometrically and hydro dynamically point of view, the efficiency value e needs to be introduced. Q represents the flowrate throughput of the centrifuge and is calculated according to 1.4. As is shown in equation 1.1 and 1.2, larger particle diameter as well as higher differences between particle and solution density increases sedimentation velocity. On the other hand viscosity is inverse proportional to u_c. (Letki, 2000)

$$\frac{\Sigma_1}{Q_1 e_1} = \frac{\Sigma_2}{Q_2 e_2} \tag{1.3}$$

$$Q_i = \Sigma_i 2 u_g \tag{1.4}$$

For upscaling purposes centrifugation experiments are performed in a lab centrifuge for which Σ factor is calculated according to equation 1.5. r_1 is the distance from the middle of the centrifuge to the liquid level of the used tube. r_2 corresponded to the distance from the middle of the centrifuge to the tip of the tube. V is the volume of the sample and ω is the angular velocity.

$$\Sigma_{Lab} = \frac{\omega^2 V}{ln(\frac{2r_2}{r_2+r_1})2g} \tag{1.5}$$

The Σ_{Tub} factor is calculated according to equation 1.6. L is the length of rotor, r_0 and r_1 correspond to the minimal, maximal radius of the centrifuge, respectively, ω is the angular speed and g the acceleration of gravity.

$$\Sigma_{Tub} = \frac{\pi L(r_0^2 - r_1^2)\omega^2}{g ln(\frac{r_0}{r_1})} \tag{1.6}$$

The Σ of the disc stack centrifuge is calculated according to equation 1.7. r_3, r_4 is the distance between rotor arbor and disc, respectively, between the outer edge of discs. N represents the number of discs, g and ω remains the same as above and θ is the angle of the discs. F_l is a factor for the non-used filtration area (see 1.8) and depends on the disc spacing. Z is the number of caulks on a disc and B represents the caulks width. (Flickinger, 2013)

$$\Sigma_{Dsc} = \frac{2\pi\omega^2}{3g} Ncot\theta(r_4^3 - r_3^3)F_l \tag{1.7}$$

$$fl = 1 - \frac{3ZB}{4\pi r_3} * \frac{1 - (\frac{r_4}{r_3})^2}{1 - (\frac{r_4}{r_3})^3} \tag{1.8}$$

Quantifying the centrifugation process is performed based on clearance efficiency (see equation 1.9). This can be used for estimation for the removal of small particle and subsequent filtration performance. The Nephelometric turbidity unit (NTU) represents a relative particle concentration in a solution and is ascertained through light scattering. (Shukla, 2006)

$$clarification\ efficiency = 1 - \frac{NTU_{centrate} - NTU_{well\ clarified}}{NTU_{feed} - NTU_{well\ clarified}} \tag{1.9}$$

1.5. Theory of homogenization

Cell disruption is needed if the protein of interest is not secreted. In the case of GFP which is expressed intercellularly, it is necessary to disintegrate the cells to release the protein. One way to establish this is high pressure homogenization. Its central element is a valve where the breakage of the cell takes part. The valve comprises a valve seat, an impact ring and the valve itself and typically consists of three regions, the inlet, the gap and the exit region. The flow is established by a piston pump. When the fluid enters the gap, which is adjustable, it reaches its highest maximum of velocity and is then flowing into the direction of the impact ring (see figure 3.1). After that it leaves the valve. In a two-stage homogenizer the fluid subsequently passes a second valve. Often it is useful to recirculate the fluid to gain higher protein release. The operating pressure depends on the device itself but can today exceed values of 150 MPa. Several theories have been estqablished to explain cell disruption (e.g.: cavitation, wall impact, turbulences). Clarke et al. (2010) concluded that shear stress is the most probable one.
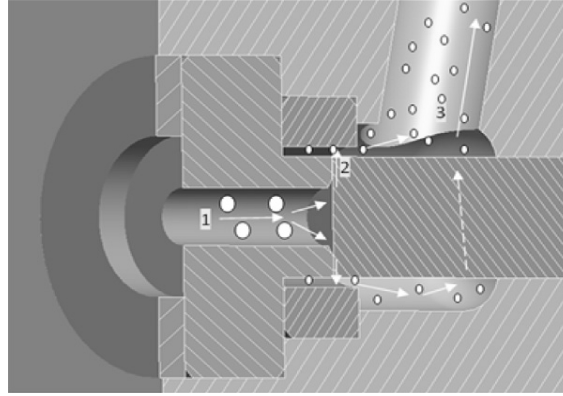
Figure 1.8.: Valve of a high pressure homogenizator with the three regions labeled. 1 = inlet region; 2 = gap region; 3 = exit region (Clarke et al., 2010)

Sauer et al. (1989) determined the homogenizer efficiency with equation 1.10. R_{max} is the maximum amount of protein available, R represents the amount of protein which is released, k is the rate constant, N the number of passages, p the pressure and α and β are constants. k α and β vary with cell type. They did a comprehensive study of the homogenization efficiency and showed that the disruption is highly dependent on the operational pressure but also, obviously, dependent on the number of passages. Furthermore, they noticed an influence of the fermentation process itself and correlated the β constant with the cell density and the growth rate μ. In their work they also mentioned that the recombinant strain was more easily to break up than the native one.

$$ln(\frac{R_{max}}{R_{max} - R}) = k \ N^{\beta} \ p^{\alpha} \tag{1.10}$$

R is determined through equation 1.11, where ϵ represents the aqueous phase volume fraction and C_P the soluble protein concentration. The subscript $_{max}$ means at 100% disruption ($R_{max} = 1$).

$$R = \frac{\epsilon_L \ C_P}{\epsilon_{L;max} \ C_{P;max}} \tag{1.11}$$

Homogenization influences all subsequent unit operations. As for example Wong et al. (1997) pointed out that a higher number of passages will lead to smaller cell debris particle. In turn, the homogenate is more difficult to clarify from debris and can also decrease filtration efficiency.
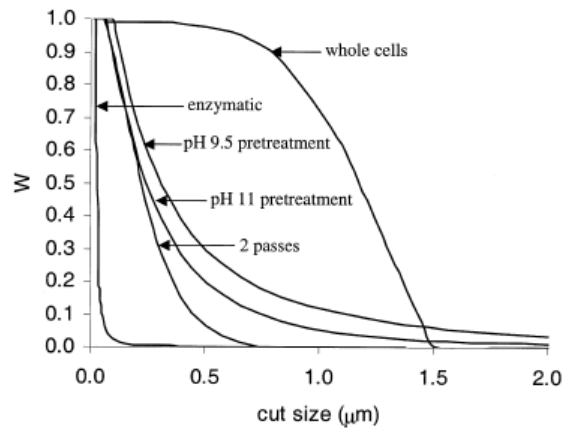
Figure 1.9.: Particle size distribution of several disruption methods and the whole cells. *W* represents the mass fraction of particles with a diameter larger than the cut size. (van Hee et al., 2004)

van Hee et al. (2004) studied the correlation between cell disruption conditions and cell debris size on *Pseudomonas putida*, a gram-negative bacteria like *E. coli*. They mentioned that pretreatment of the cell broth, enhancing the pH with ammonium hydroxide, have an effect on the debris size distribution (see figure 1.9), due to the destruction of muramic acid. The results were also compared to an enzymatic disruption technique.

High pressure homogenization is one of the disruption techniques which exhibit the highest yield. The big disadvantage is its lack of selectivity. But for periplasmatic located products a selective release can be achieved by a combination with a heat lysis. Despite this fact it is still a widely used method at process scale level. (Balasundaram et al., 2009)

Homogenization seems to be one of the most sensitive unit operations in downstream processing. To ensure a proper purification process it is inevitable to know and use the right operational parameters.

1.6. Preparative ion exchange chromatography (IEX)

1.6.1. General

Liquid chromatography is a general term for a process where a stationary phase is interacting with a solute which is carried by a mobile phase. Those interactions ensure the separation of a mixture of substances if its components interact differently. There

11
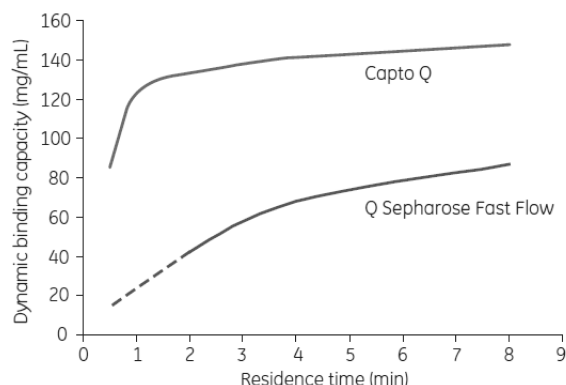
Figure 1.10.: Dynamic binding capacity of bovine albumin serum (BSA) as a function of residence time of CaptoQ and Q-Sepharose FF (GE Healthcare Life Sciences, 2014a)

a different modes of operation and mechanism of how the components can interact with the stationary phase. Proteins possess a net charge due to the fact they comprise different acidic and basis amino acids. Dependent on the pH they are positively, negatively or neutral net charged. The isoelectric point of a protein (IP) is the pH, where the net charge is zero. For ion exchange chromatography the pH should be at least 1 pH distant to its IP. If the charged protein come into contact with counter ions immobilized on a matrix a reversibly binding occurs. Different ligands are available distinct in cation or anion and weak or strong exchanger. Strong and weak are related to protonation properties. (Gorgio Carta and Jungbauer, 2010)

In this work, CaptoQ and Q Sepharose Fast Flow were used. The ligands of both, represented through the Q letter, are a quaternary amine ($R - N^+(CH_3)_3$), which is a strong anion exchanger. The matrixes of both are natural carbohydrate polymers. CaptoQ is a highly cross linked agarose with a dextran surface extender and Q-Sepharose FF matrix consist of a 6% highly cross linked agarose. Dextran surface extender extends the mass transfer properties and increases capacity. This should provide a higher dynamic binding capacity over a wide range of residence times. In comparison Q Sepharose FF had been used over decades, is well-documented and reliable. In figure 1.10 both resins are compared. It is obvious that CaptoQ exhibits a higher capacity due to its dextran surface extender. (GE Healthcare Life Sciences, 2014b; GE Healthcare Life Sciences, 2014a)

Some features of such natural carbohydrate polymers are low solid densities, limited mechanical strength and chemical resistance to cleaning in place (CIP) procedures. The physical shape of the agarose beads is spherical. (Gorgio Carta and Jungbauer, 2010)

1.6.2. Single component chromatography

Ideal chromatography is described by local equilibrium theory. Here, the performance is only dependent on the velocity and adsorption equilibrium. However, in reality band-broading mechanism, due to adsorption rate limitations and dispersion are occurring and decreasing column efficiency. Many efforts have been made to enhance the predictability of chromatography performance by mathematically modeling. The common models can be divided into plate-, rate- and stochastic models. The first one segments the column into discrete zones. The rate model takes kinetic effects into account and describes non-equilibrium conditions. The latter one is less common in preparative chromatography. Modeling is essential to, among others, design new sorbents, improve and validate existing processes as well as developing new ones. (Jungbauer, 1996; Gorgio Carta and Jungbauer, 2010)

G. Carta et al. (2005) mentioned that process performance of IEX resins are dependent on equilibrium and rate factors. The former one is determined by the type and concentration of the ligand, the accessible surface and also by the base matrix, the latter one by mass transfer effects. This is affected by external film resistance (phase velocity) and by intraparticle transport, which is associated with molecular diffusion. In general, protein chromatography is controlled by mass transfer. Different methods are available to gain information about intraparticle diffusivities categorized into macroscopic and microscopic approaches.

As mentioned above adsorption on porous particles is mostly dependent on diffusional properties. There are distinct mass transfer characteristics which influence adsorption. The *external film mass transfer* describes the diffusion of a protein from the surrounding liquid to the particle surface. It is independent on product concentration unless the viscosity of the solution is not changing and decreases with smaller particle size and higher fluid velocity. Except for low concentrations, film mass transfer is mostly negligible in preparative applications. *Pore diffusion* occurs if the solute is small enough to enter the pore and resist the attraction of the force field of the pore surface. Its driving force is the concentration gradient of the solute within the pore. This diffusivity is normally lesser than that in an unhindered diffusion and is caused by steric hindrance together with tortuosity. Furthermore, already adsorbed proteins on the pore wall influence the diffusivity. *Solid diffusion* describes the transport without detachment of the adsorbent. Its driving force is the concentration gradient of adsorbed solute in the stationary phase. At wide pores and high binding strength the most influencing mechanism is *pore diffusion*. (Hahn, 2012)

The dynamic binding capacity (DBC), defined as the capture efficiency at breakthrough (usually at 5% or 10%), is the most important characteristic value when it comes to preparative approaches. This value can be easily determined by applying a protein solution under a fixed flow rate onto a column until breakthrough occurs.
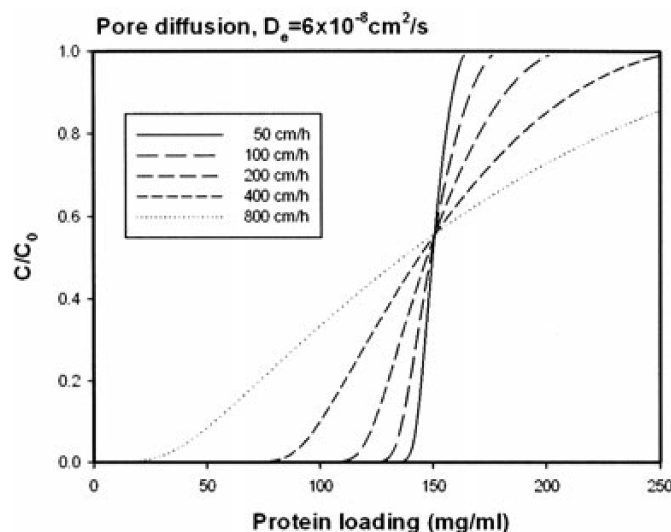
Figure 1.11.: Break through curves for a pore diffusion control in a column system under different velocities. D_e is the pore diffusion coefficient. (Hahn, 2012)

The shape of a break through curve is dominated by the adsorption isotherm and effective diffusivity. In figure 1.11 is a typical BTC shown. As it can be seen a lower linear flow rate results in a steeper curve and a higher dynamic binding capacity. This behavior is similar also for other mass transfer mechanism. (Hahn, 2012)

Hashim and Chu (2007) showed that by using the simplified Thomas solution, known as the Bohart-Adams equation, it is possibly to predict the breakthrough behavior of a single component system.

1.6.3. Determine equilibrium constants through adsorption isotherms and -kinetics

Adsorption of proteins is complicated and difficult to predict through a precise model. For instance, complicating factors are the heterogeneity of macromolecules, diffusional resistance, local and global unfolding events. Therefore (semi-)empirical attempts are needed and then can be correlated by using isothermal models. In 1.12 the Langmuir equation for a single component isotherm is shown. This non-linear model describes the amount of adsorbate over the supernatant concentration. For IEX it is a rectangular function which becomes less favorable at higher salt concentrations. K is referred to as the equilibrium constant, q_m is the maximum binding capacity given in $\frac{mg_{protein}}{mL_{resin}}$ and q_i is defined as the adsorbed protein concentration, also given in

$\frac{mg_{protein}}{mL_{resin}}$ at a given C_i which represents the supernatant concentration. If C approaches 0 the isotherm becomes linear. (Gorgio Carta and Jungbauer, 2010)

$$q_i = \frac{q_m K C_i}{1 + K C_i} \tag{1.12}$$

The Langmuir model does not take heterogeneity of the adsorption sites and also interaction between adsorbed species as well as multilayer adsorption into account. Additionally, it is contradictory to the second law of thermodynamic. Practically, for solid/liquid adsorption processes the equation is only applicable at low concentrations. This is caused by the fact that calculation is done with the absolute adsorbed amount rather than with the excess one. (Tóth, 2003)

Hahn (2012) mentioned an easy way to determine the adsorption isotherm in small scale and to design the process over a wide range of concentration.

Giorgio Carta (2012) developed a simple calculation of DBC at any point out of the equilibrium binding capacity (EBC), if it is assumed that intraparticle mass transfer is controlled by pore diffusion and the isotherm is rectangular. Hence, the ratio $\frac{DBC}{EBC}$ depends on the residence time and is independent of feed concentration.

The adsorption of proteins as a function of time in spherical particles can be described by rate equations. All of them are related to specific control mechanism, like for example pore diffusion, kinetic resistance and the linear driving force model. (Gorgio Carta and Jungbauer, 2010)

Adsorption kinetics can be verified in different ways as it is proposed by Hahn (2012). The simplest method is to suspend particles with the protein solution, stir it and draw samples after specific time intervals. A more complex way is to make the uptake visible by confocal laser scanning microscopy (CLSM). This allows observing the intraparticle transport, discriminating between pore and surface diffusion, enabling the possibility of direct determination of effective diffusivities and examining individual particles.

Another optical method was introduced by Stone and Giorgio Carta (2007). They used the difference in the refracting index of protein loaded and protein free regions of the particle to make the solute transport observable with a simple microscope (see figure 1.12). The migration of the adsorption front can be described by the so called *shrinking core model* and is believed to be the dominant mechanism in intraparticle transport in macro porous media.

Yang and Sun (2007) developed a sophisticated model to describe the intraparticle transport of proteins in porous media (see figure 1.13). The so called structured
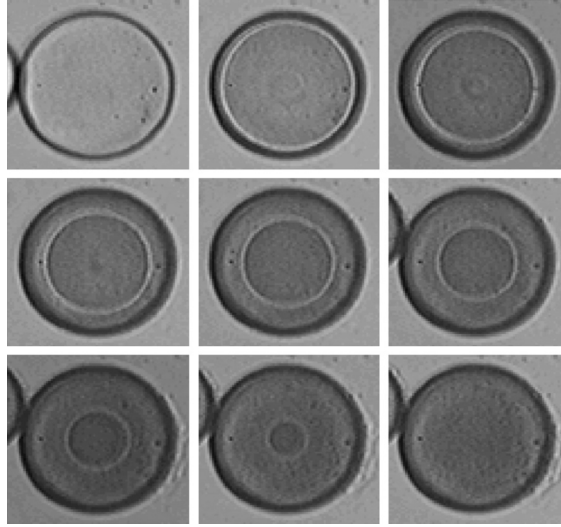
Figure 1.12.: Adsorption of lysozyme from a 2.0 $\frac{mg}{mL}$ solution. Time interval of the images is 5 min incrementing up to a total of 40 min. The adsorption front which is migrating towards the center is clearly visible. (Stone and Giorgio Carta, 2007)
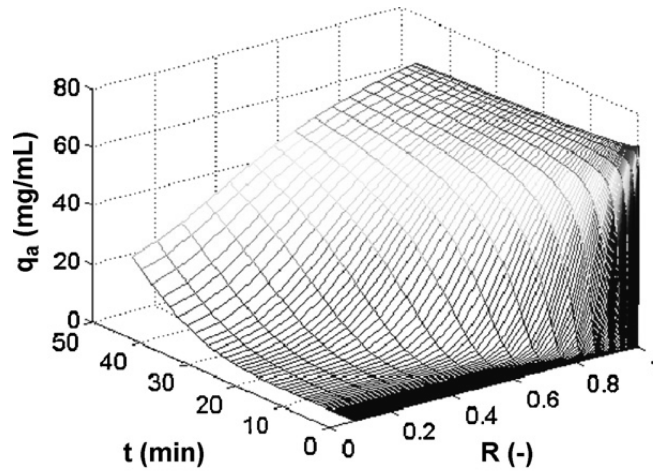
Figure 1.13.: Simulated intraparticle concentration profile of adsorbed γ-globulin with a feed concentration of 1.8 $\frac{mg}{mL}$ on an anion exchange resin. R represents the normalized radius of the particle. (Yang and Sun, 2007)

parallel diffusion model (SParD) takes into account many different effects such as the shrinking core and pore size distribution.

In the last decades a lot of simulation and modeling work of single component protein chromatography has been done. Chromatography of a single component is in most, if not in all cases, far away from reality. In biotechnology processes multicomponent solutions are the standard.

1.6.4. Multi component adsorption behavior

In all chromatography purification strategies, it is common to separate at least two components from each other. In IEX there are three possibilities how those elements can behave. First, the net charge of one component is neutral, the other is positive or negative, respectively, and will bind to the column. Second, both components bind to the column but these isotherms are linear. In those both cases the two components will not, or rather negligibly, be influencing each other and can be handled as a single component system. In the third case, both bind and at least one isotherm is nonlinear. Here, a competitive binding occurs. Depending on the equilibrium constant and the maximum binding capacity a displacement of one component will occur.

Skidmore and Chase (1990) showed that the prediction of such a system was more accurately with a full competitive model as with the non-competitive ones. They used the variable θ, which is a dimensionless value from 0 to 1 and represents the fraction of occupied sites on the adsorbent, for the derivation of the multi component Langmuir isotherm (see equation 1.13). q_i^* represents the binding capacity from component i at a sorbent concentration in the liquid phase c_i^* at equilibrium, q_{mi} is the maximum binding capacity of component i and K_{ai} is the adsorption constant of that component. Discrepancies from their model to the observed data were explained by protein size, protein-protein interaction and as well as the thermodynamically inconsistency (violating Gibbs-Duhem relationship) had not been taken into account. Broughton (1948) noted, admittedly for gas mixtures but the meaning is still the same, that the binary Langmuir isotherm is only consistent if $q_{m1} = q_{m2}$ and no displacement occurs. Only then, the second law of thermodynamics is fulfilled.

$$q_i^* = \frac{q_{mi} K_{ai} c_i^*}{1 + \sum_{j=1}^{n} K_{aj} c_j^*} \tag{1.13}$$

Gu et al. (1991) suggested that adsorption with uneven saturation could be affected by size exclusion and or chemically induced effects. Therefore they introduced the discount factor δ, which is the ratio $\frac{q_{m1}}{q_{m2}}$ and ranges from 0 to 1. Equations 1.14 and 1.15 represent the extended competitive Langmuir equation for displaced and replaced

components, respectively. If the saturation capacities are equal then those equations are reduced to the common competitive Langmuir isotherm (see 1.13). Isotherm crossover can occur at 2 component systems. This can indicate a change in selectivity, followed by peak reversal and crossover breakthrough curves phenomenon.

$$q_1^* = \frac{K_{a1}c_1^*[(1 + K_{a2}c_2^*)q_{m1} - \delta K_{a2}c_2^*q_{m2}]}{1 + K_{a1}c_1^* + K_{a2}c_2^* + (1 - \delta)K_{a1}c_1^*K_{a2}c_2^*} \tag{1.14}$$

$$q_2^* = \frac{K_{a2}c_2^*[(1 + K_{a1}c_1^*)q_{m2} - \delta K_{a1}c_1^*q_{m1}]}{1 + K_{a1}c_1^* + K_{a2}c_2^* + (1 - \delta)K_{a1}c_1^*K_{a2}c_2^*} \tag{1.15}$$

Garke et al. (1999) showed that the extended Langmuir isotherm was predicting both components at different mass fractions rather correctly. The smaller component with a higher binding constant was almost not affected by the second larger component.

Understanding the uptake of proteins in ion exchange media is crucial for process design. For this reason, G. Carta et al. (2005) established a model for two component adsorption on porous ion exchange media. The shrinking core model was able to predict the rates correctly, for simultaneous and sequential adsorption, respectively. The diffusivities of the used components were derived from single component batch uptake curves. The component with the higher binding strength displaced the other one, which adsorption behavior resulted in an overshoot above equilibrium. The magnitude of the overshoot was dependent on the feed concentration (see figure 1.14). Furthermore, they visualized the intraparticle adsorption behavior explaining how the overshoot above equilibrium of the weaker bounded component was established.

Traylor et al. (2011) improved this model to calculate the chromatographic breakthrough of a binary system. They mentioned that it is helpful to separate the adsorption process into three zones. Zone 1 is where both components are simultaneously being adsorbed and the second one is displaced. In Zone 2 B is adsorbed to its maximum but is completely displaced by A. The third Zone is the one where adsorption of A is not hindered by B. They proved there model with experimental data and also proposed a mechanism of the adsorption behavior in the column. (see figure 1.15).

1.7. Master thesis objectives

This master thesis shall provide an insight on specific downstream process units. Homogenization of *E. coli*, centrifugation and capturing of the recombinant protein with anion exchange chromatography will be characterized. Homogenization will
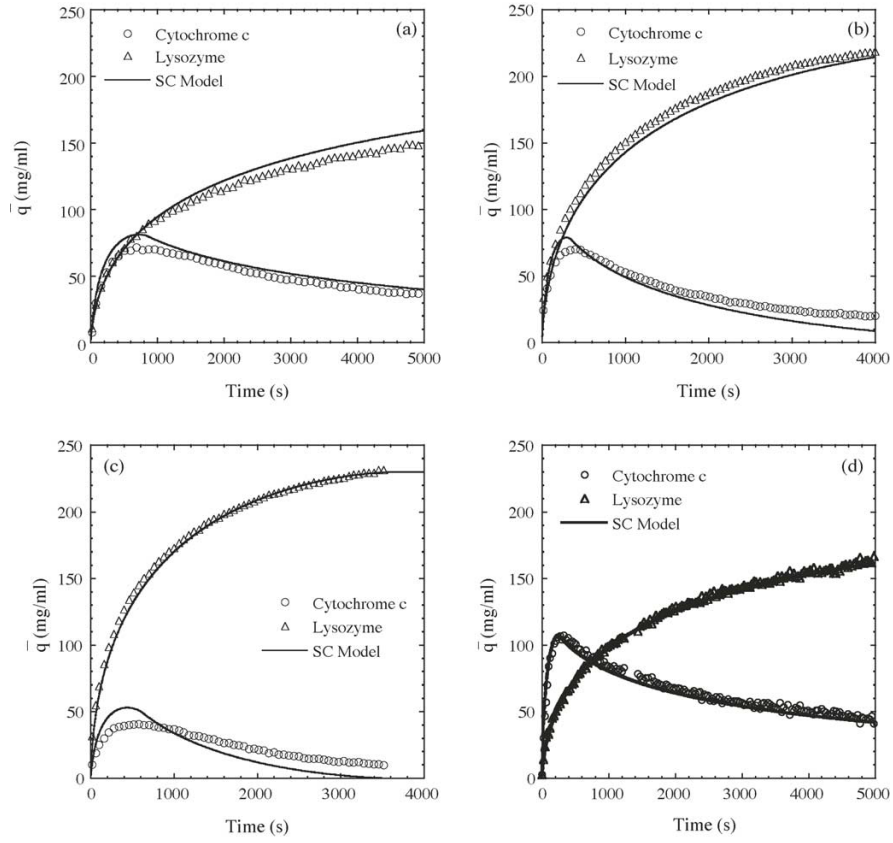
Figure 1.14.: Simultaneous batch adsorption experiments of Lysozyme/Cytochrome C at different feed concentration. SC = shrinking core model. (a) 0.5/0.5 $\frac{mg}{mL}$, (b) 1.0/1.0 $\frac{mg}{mL}$, (c) 1.5/0.5 $\frac{mg}{mL}$, (d) 0.5/1.5 $\frac{mg}{mL}$. (G. Carta et al., 2005)
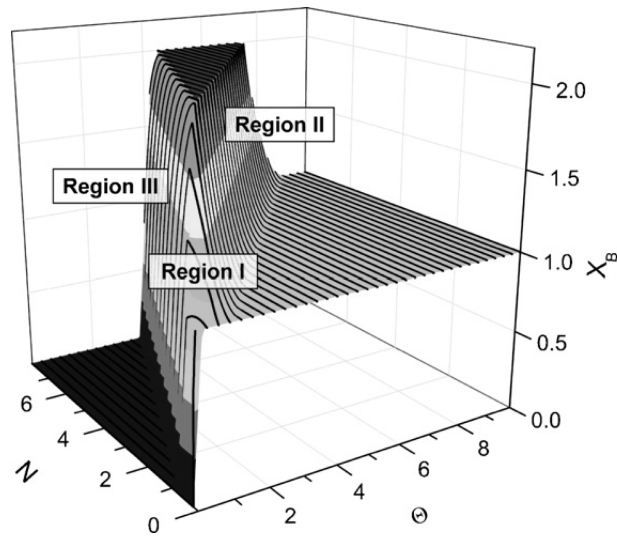
Figure 1.15.: Normalized mobile phase concentration (X_B) of component B as function of dimensionless time (Θ) and dimensionless axial column position (N). (Traylor et al., 2011)

be thoroughly investigated to understand which variables are influencing the performance. Multicomponent adsorption on ion exchange will be another mayor part of this thesis.

2. Material and Methods

2.1. Material and Devices

In 2.1 the used materials are shown and used devices are listed in table 2.2.

Table 2.1.: List of used material

Unit operation	Material / Chemical	Lot-No / Order No	Company
Analytics	Agilent Bio SEC-5 guard Column	USDMG01085 / 5190-2530	Agilent Technologies, Inc.
Analytics	Agilent Bio SEC-5 Main Column	USDMF01086 / 5190-2528	Agilent Technologies, Inc.
HIC	Butyl Sepharose High Performance	- / 17-5432-03	GE Healthcare Bio-Sciences AB
IEX	Capto Q	10070381 / 17-5316-03	GE Healthcare
Misc.	Hydrochloric acid 25%	z268212 224 / 1.00312.2500	Merck KGaA
Analytics	Mini-Protean® TGX™ Gels	- / # 456-1095	Bio-Rad Laboratories, Inc.
IEX	Q-Sepharose FF	10021699 / 17-0510-04	GE Healthcare
UF/DF	Sartobran P Sartocon Hydrosart 10 kD Casette 0.6 m²	- / 3021443906E–SW	Satorius Stedim Biotech GmbH
Misc.	Sodium chloride for analysis	K44555504 332 / 1.06404.500	Merck KGaA
Misc.	Sodium hydroxid 99.9 %,p.a.	373201621 / 6771.2-16P	Carl Roth GmbH + Co. KG
SEC	Superdex 75 prep grade	10046124 / 17-1044-04	GE Healthcare

UF/DF	Pellicon/r XL Filter 10 kDa 50 50 cm²	C9PN61321 / PXC010C50	Merck Millipore
Misc.	TRIS Pufferan 99.9%, p.a.	233196559 / 4855.300	Carl Roth GmbH + Co. KG
Misc.	Tween® 20 Polyethylene glycol sorbitan monolaurate	SZBD2190V / P1379-1L	Sigma-Aldrich Co.

Table 2.2.: List of used devices

Unit operation	Device	Serial & Inventory No.	Company
Chromatography	ÄKTAexplorer System	01158062 / DS-GTCS02GH	GE Healthcare
Chromatography	ÄKTAexplorer Frac-950	01155646	GE Healthcare
Chromatography	ÄKTApilot	1689672	GE Healthcare
IEX	AxiChrom 100/300 & 100/500	-	GE Healthcare
Analytics	Carry 60 UV-Vis G6860A	MY13480019 / 1682	Agilent Technologies
Centrifugation	Centrifuge 5415R	-/1124	Eppendorf
UF/DF	Cogent© μ-Scale TangentialFlowFiltrationSystem	U0013 / 1102	Milipore
Centrifugation	Disc stack centrifuge	1729-791	GEA westfalia seperation Technology GmbH
Centrifugation	Heraeus Contifuge Stratos Centrifuge	41576127	Thermo Fisher Scientific
Homogenization	Homogenizator Ariete NS3600	10185	GEA Niro Soavi
Homogenization	Homogenizator Panda	8204	GEA Niro Soavi

Analytics	HPLC Agilent 1100 series with DAD and FLD	- / HP1100B	Agilent Technology, Inc.
infinte M200Pro	1305004737/1514	Tecan	
Centrifugation	Labcentrifuge Sigma 2-16P	122109 / 095723	Sigma
Analyitcs	Mini-Protean$^{\circledR}$ Tetra System	552BR 113608 / -	Bio-Rad Laboratories, Inc.
Analytics	Portable Turbidimeter 2100Q	13100C028466	HACH
Analytics	PowerPac^{TM} Basic	041BR114202 / -	Bio-Rad Laboratories, Inc.
Analytics	Precision Cells SUPRASIL 10 mm	104.002-QS	Hellma
rotator SB3	R110002435	Stuart	
UF/DF	Sartoflow$^{\circledR}$ Advanced	7SZB − 0041	Satorius Stedim Biotech
HIC	Sepacor 90/300	940072/2	Sepacor Inc
Chromatography	Tricorn 50/500	-	GE Healthcare
Analytics	Viscosimeter LVDV-II+ Pro CP	8561662	Brookfield
Filtration	Zero-T System	-	Satorius Stedim Biotech

2.2. Methods

2.2.1. Fermentation

The used *E.coli* strain for the fermentation process was HMS174(DE3) with the plasmid pET11a-GFPmut3.1 with the resistance marker Ampicillin. The fermentation process was designed as a fed-batch culture. Cultivation was done at 37 °C, pH of 7 and a pO$_2$ of 30%.

At the beginning was the batch process. When the whole glucose was consumed by the bacteria, the exponential feed started. The rate was adjusted to a growth rate μ of 0.1 h^{-1}. This was done for 3 cycles of generations (around 21 h). After that a final cell density of approximately 27 $\frac{g_{DCW}}{L}$ was established. With 20 $\frac{\mu mol}{g_{DCW}}$ IPTG the cells got

Table 2.3.: System specs for infinte M200 Pro measurments

System specs	value
Excitation wavelength	485 nm
Excitation bandwidth	9 nm
Emission wavelength	520 nm
Emission bandwidth	20 nm
Sample volume	100 μL
Gain	50 Manual
Number of flashes	40
Integration time	20 μs
Lag time	0 μs
Settle time	0 μs
z-postion (Manual)	15 475 μm
Mode	Fluorescence Top Reading
System	AIAM-ITX-216
used well plate	Nunclon 96 Flat Bottom Black Polystyrol LumiNunc FluoroNunc

induced to produce the recombinant GFP for around 7 h. The scale of the process was varying from around 20 to 100 L.

2.2.2. Homogenization

Homogenization was performed at different cell densities (20 to 90 $\frac{gDCW}{L}$), pressures (250 to 900 bar) and passages (1 to 3). Turbidity and viscosity at a sheer rate of 150 s^{-1} was measured. The GFP concentrations of the clarified homogenates were determined with the Tecan reader.

2.2.3. Adsorptionisothermes and -kinetics

The pipetting scheme for the isotherms were calculated according to equation 2.1 and 2.2, where V_g is the volume of the gel in a specific slurry, V is the overall volume, V_s describes the needed sample volume, c_0 is defined as the sample concentration which is used, c_i is the expected concentration of the supernatant, q_i is the expected binding capacity and x represents the used concentration. The used volume was 1 mL and the slurry was 50%.

$$V_g = \frac{c_0 V - c_i V}{c_0 + x q_i} \tag{2.1}$$

$$V = V_g + V_s \tag{2.2}$$

For every estimated c_i the q_i value was computed according to equation 1.12. Adsorption constant K_i and the maximum binding capacity qm were assumed in consideration of the pure GFP isotherm. At first, the resin was washed with buffer. Then the slurry concentration was adjusted to 50%. The resin and sample were pipetted in a 1.5 mL reaction tube, vortexed and attached for 24 h on the rotator (speed step: 8). Then the tubes were centrifuged with the eppendorf centrifuge (13.2 rpm for 1.5 min) and the fluorescence was measured with the Tecan reader (detailed specs see 2.3).

For the determination of the adsorption kinetics it was considered that the change in the initial supernatant concentration had to be negligibly small. But on the other hand high enough to measure the decrease in the fluorescence signal seriously. The sample and a small amount of resin were pipetted into a 15 mL tube. Subsequently after adding the resin a timer was started and the tube placed on an end over end. Samples were drawn in specific time intervals and measured.

2.2.4. Column packing

For small scale columns, washed resin (50% slurry) was pipetted into a clean Tricorn column with a reservoir on top of it, and then the top plug mounted and subsequently attached to the Äkta explorer system. The column outlet was not mounted to the system. Beginning with a low flowrate (0.5 $\frac{mL}{min}$) and cautiously increasing until the pressure limit of the resin is reached. Then it was remained at that flowrate for 15 min. Next that reservoir was removed, pre wetted filter was put on top of column and the top plug was mounted. The top was slowly turned down until the stamp was close before contacting the upper level of the resin. The column was completely attached to the system, consequently also the bottom outlet of the column. As before the flowrate was slowly raised until pressure maximum of the resin was reached and then under this volumetric rate remained for approximately 10 min. Then, the top was cautiously turned down until the stamp reached the bed surface. Test of the column performance had been done by injecting 25 μl of 0.8 M NaCl solution with a 0.4 M NaCl solution as a running buffer.

Large scale columns were packed and tested according to the GE text instructions.

2.2.5. Multicomponent adsorption experiments in a column

Determination of multicomponent adsorption behavior in a column was performed in small scale. 1 mL Q-Sepharose FF and CaptoQ columns were packed and used for the experiments (packing instructions see 2.2.4). Due to the fact that this effect is time depended, the runs were performed at different residence times, different load volumes and GFP concentrations. The only difference to the pilot scale method was that the wash out was done in 5 CV instead of 2 CV. For offline fluorescence measurements (see table 2.3) the flow through, wash out and the elution steps 1 and 2 were collected.

2.2.6. Current standard protocol for purification of recombinant GFP in pilot scale

Following protocol is a detailed procedure for the purification of recombinant GFP from *E. coli* in pilot scale. If not mentioned differently, all processes are performed at room temperature and ambient pressure (+20 °C).

Cell broth must be centrifuged with the disk stack centrifuge at 13 650 rpm with a flow rate of 60 $\frac{L}{h}$ to harvest the cell pellet. This is suspended in a chilled (+4 °C) solution of 10 mM Tris 0.1 M NaCl and 0.1% Tween 20 adjusted, with a 25% HCl to a pH of 7.5 to reach a cell density of 25 $\frac{gCDW}{L}$. Cell disruption is performed with a Panda 2-stage high pressure homogenizer at 750 and 70 bar, first and second stage respectively, in two passages. Cell debris separation is done in the disc stack centrifuge at 13 650 rpm with a flowrate of 30 $\frac{L}{h}$. The clarified supernatant is filtrated with Sartoquard PES (1.2 / 0.2 μm) filter. It is recommended to perform filter tests with the Zero T in advance. Diafiltrating is established with the Sartoflow Advanced with a Hydrosart 10 kDa membrane (0.6 m²) within 5 volume changes. DF-buffer is a 10 mM Tris buffer at a pH of 7.5.

Capturing of the protein is done with the ion exchange chromatography (IEX) with the Q-Sepharose FF resin at a residence time of 4 min. The resin will be packed in an Axichrom 100/300 with a bed height of approximately 16.5 cm. Running buffer (Buffer A) is a 10 mM Tris adjusted to a pH of 7.5 and elution buffer (Buffer B) is a 10 mM Tris , 1 M NaCl also at a pH of 7.5. WashOut is done within 2 column volumes (CV). Elution is done as a step gradient with 5% of buffer B in 3 CV, 30% in 3 CV and 100% in 5 CV.

Then the IEX eluate must be salted up to 3.3 M with a 5 M NaCl solution. Intermediate purification is then performed with the Butyl Serpharose HP, a hydrophobicity interactive chromatography (HIC), which will be packed in a Sepacor 90/300 column.

The bed height was about 15.5 cm. The flow rate is about 90 $\frac{cm}{h}$. Here, the running buffer (Buffer B)is a 10 mM Tris with 3.3 M NaCl at a pH of 7.5. Buffer A remains the same as before. The duration of the wash out step is about 2 CV.

The last step is done with a size exclusion chromatography (SEC). This will be packed in an Axichrom 100/500 with a Superdex 75 resin of a bed height of 40 cm. Amount of loading is approximately 3% of the column volume. It is operated by a linear velocity of 30 $\frac{cm}{h}$. The running buffer is a phosphate buffered saline (PBS) buffer (recipe is obvious at appendix B).

To ensure product quality during downstream processing viscosity at sheer rate of 150 s⁻¹ is measured from the cell suspension and the homogenate. Solid content must be quantify with the lab centrifuge from cell suspension and homogenate. For that reason a volume of 10 mL must be taken and centrifuged for 40 min at 4000 rpm. Turbidity must be measured from the homogen cell suspension, homogenate, cleared supernatant, after filtration and from the diafiltrate retentate.

The purified GFP must be analyzed by HPLC with a BIOSEC5 300 Angstrom at a flowrate of 0.3 $\frac{mg}{mL}$. Diode array detector (DAD) is used to measure a spectrum from 250 nm to 550 nm. Finally as a quality standard the ratio of $\frac{280}{490}$ must be determined with the photometer using a precision cell cuvette.

3. Results and discussion

3.1. Centrifugation of the cell broth

Due to the fact, that a multitude of fermentation broths were used, it was necessary to keep the cell separation almost constant. So that variances of the measurements only could be related to the fermentation itself.

At first some lab scale tests were made to reveal the clarification efficiency of the cell broth. This was done by the Bio Process Engineering exercise group in February, 2014. They, under supervision of Rainer Hahn and Bernhard Sissolak, determined the μ factors of the lab, contifuge and disc stack centrifuge.

The calculated parameters are shown in table 3.1.

Table 3.1.: Calculated μ factors

Centrifuge	μ
Lab-centrifuge	1
Contifuge	0.23
Disc stack centrifuge	0.2

With those correction factors it is possible to use the centrifuge at the same operating conditions with respect to separation efficiency. Hence, this variable could now be regarded as constant.

3.2. Homogenization performance

3.2.1. Protein release and disrupted fractions

Figure 3.1 shows a logarithmic form of the protein release as a function of pressure. The parameters k and α were determined by fitting data of the first passage according to equation 1.10. The parameter β was calculated through fitting the first and second passage.

3. Results and discussion
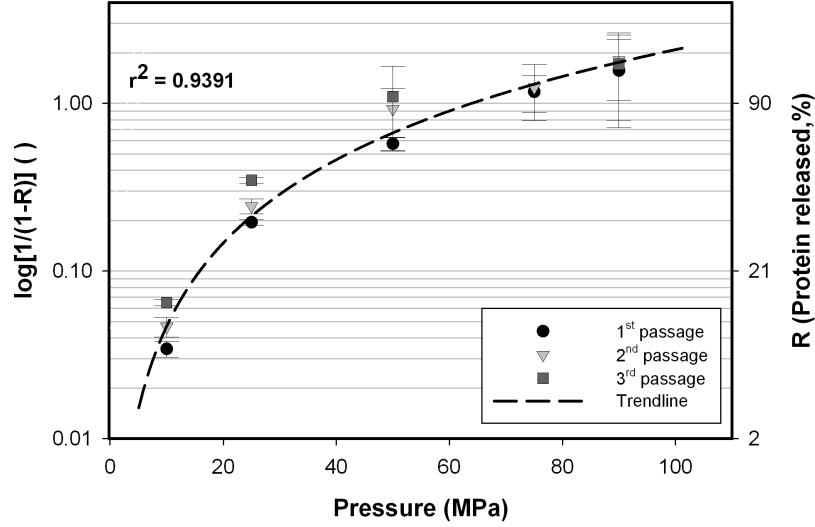
Figure 3.1.: Disrupted fraction in logarithmic scale as a function of pressure according to equation 1.10. All three passages are shown regardless of there biomass concentration.

- reaction constant $k = 1.05 * 10^{-3}\ MPa^{-\alpha}$
- $\alpha = 1.65$
- β has almost no effect at all. It can be assumed that $\beta \sim 0$

In equation 3.1 the used fit, and its calculated constants, is shown. P is the used pressure, N the number of passages and R represents the normalized amount of protein which is released. R_{max} is the maximum amount of protein which can be released and is set to 1. In most cases R_{max} is determined as the measured protein in the supernatant at 90 MPa after the second passage.

$$log(\frac{R_{max}}{R_{max} - R}) = 1.05 * 10^{-3}\ MPa^{-\alpha}\ N^0\ P^{1.65} \tag{3.1}$$

Although, under 50 MPa the influence of the number of passages is evident, additional passages do not have an dramatic impact on protein release. The maximum increase was about 10% after the third passage. This led to the point to set the β value to 0. Above 50 MPa, homogenization performance was hugely satisfactorilyafter one passage.

About 150 up to 200 $\frac{mg}{g_{DCW}}$ of soluble GFP and about the same quantity in inclusion bodies were produced by the cells. This means that at maximum almost 40% of the cell was comprised of the recombinant protein.
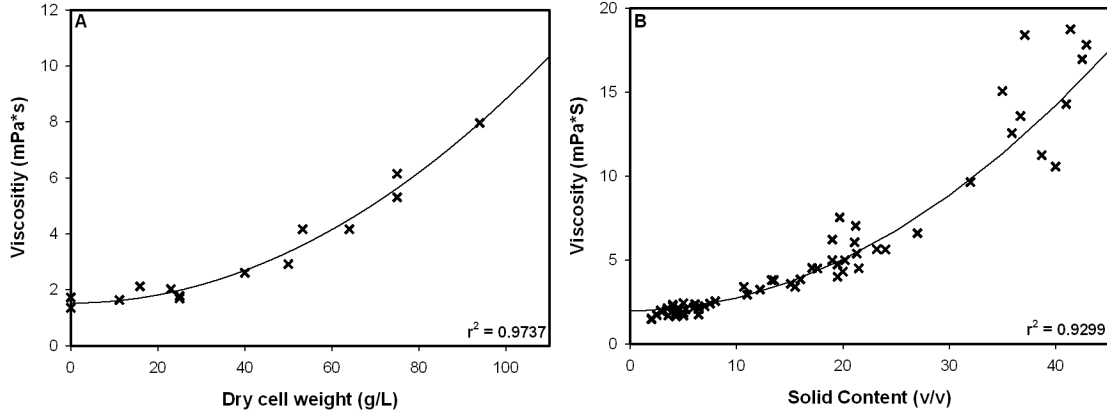
Figure 3.2.: Viscosity dependency of A) cell suspensions before homogenization as a function of adjusted dried cell weight and B) homogenates with minimum of 50% protein release as a function of measured solid content. Correlation factor and fitted curves according to equations 3.2 are shown in the plots. Viscosity measurements were done at a sheer rate of $150\,s^{-1}$.

3.2.2. Viscosity

Figure 3.2 shows the dependency of viscosity on the solid content of cell suspension and homogenates. It was possibly to establish a nonlinear correlation of those variables with a modified form of the Vand equation (see equation 3.2). Accordingly, an increase in the cell density and solid content, respectively, will lead to an increase in the viscosity. μ_L represents the viscosity of the buffer and ψ is the solid content.

$$\mu = \mu_L * (1 + \frac{\psi^2}{2100})\ for\ cell\ suspensions$$
$$\mu = \mu_L * (1 + \frac{\psi^2}{258})\ for\ homogenates$$

(3.2)

In this plot only values with a specific release of protein and at pressures above 50 MPa were used. The viscosity of the cell suspensions itself were at a lower level than those of the homogenates. Especially at higher cell densities below pressure of 50 MPa the viscosity measurements were distorted. It was assumed that at this operational region almost intact DNA was released. At a second passage or even at higher pressure the viscosity decreased.

$$y = 0.55 * x - 1.42$$

(3.3)
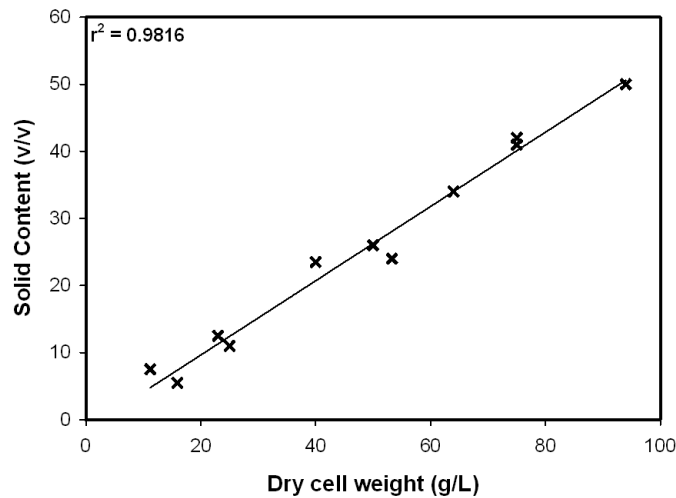
Figure 3.3.: Dry cell weight as a function of the determined solid content. The correlation factor and the trend line are shown in the plot.

The correlation of solid content to cell density is shown in figure 3.3 and in equation 3.3. Apparently, the more cells were suspendend in the process solution, the higher the solid content in the solution. After a certain point, small changes in the adjusted cell suspension have a huge effect on the viscosity. This in turn will lead to problems in the subsequent downstream process steps, i.e. centrifugation and filtration. Therefore it is necessary to run the process in the linear range of this correlation to establish a stable operating protocol.

3.2.3. Clearance efficiency and cell debris separation

Reaching a high protein release is one aspect of the homogenization performance. Another one is to clarify the homogenate from debris at a sufficient level, afterwards by centrifugation (e.g. disc stack centrifugation). This step mainly depends on particle size and viscosity. The latter one was discussed above. Determination of the particle size was not carried out. Instead, it was determined indirectly by measuring the turbidity of the solution. This revealed following trends:

- Cell suspensions before homogenization had always higher turbidity than the homogenates
- The higher the cell density of the suspension the higher the turbidity
- The higher the operational pressure the lower the turbidity of the homogenates

- Mostly, cleared cell suspensions before homogenization revealed the lowest turbidity
- Mostly, cleared homogenates revealed at higher cell density lower turbidity values
- The more passages were performed the lower was the turbidity

Those trends above pointed all to the fact, that:

$$Turbidity \propto \frac{1}{d_{particle}} \tag{3.4}$$

Determination of the turbidity was performed by measuring the amount of light which is scattered in a $90°$ angle from the light source through the particles in the solution. Evidently, the more particles are present in the liquid, the higher is the turbidity. This effect was seen at the cell suspension before homogenization. However, this is only true if the particle size remains constant.

In fact, during homogenization the particles got smaller with ongoing passages and increasing operational pressure. Despite the fact, that more surface area was created by smaller particles, also more light was scattered by coincidence and therefore more photons had reached the detector.

In lab-scale experiments following trends had been carried out:

- The higher the cell density the greater the clearance efficiency
- The higher the pressure the lower the clearance efficiency

In figure 3.4 the clarification in dependence on the dried cell weight and the operational pressure is shown. Although, a different strain had been used the effect is still the same.

Overall, the clearance efficiency was determined by the operating parameters of the homogenization step. Accordingly, performance was enhanced by a higher cell density and lowering the operational pressure.

Optimization of the homogenization step is crucial. If the clearance efficiency is low, then huge areas of filtration membranes are needed.

The disc stack centrifuge is a continuously working device. After a certain point the centrifuge needs to be discharged to get rid of the accumulated cell debris pellet. It was determined that at each discharge of the pellet around 0.3 L to 0.4 L of supernatant was also released. For that reason the pellet compression characteristics of different homogenates were investigated. Suspensions with different cell density were homogenized at 70 MPa. The solid contents of the cell suspensions and the homogenates were determined. The reduction factor was estimated as the ratio of compressed cell
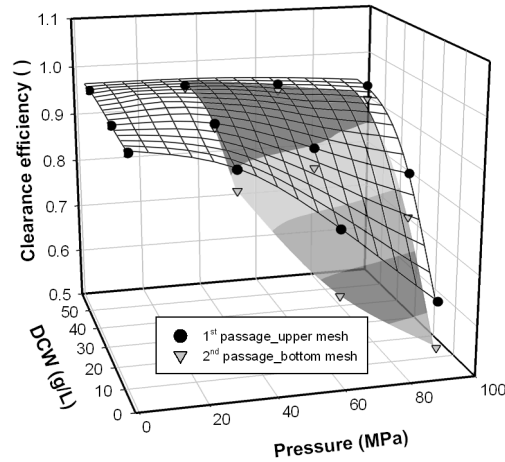
Figure 3.4.: Clearance efficiency as a function of dry cell weight and operational pressure. In this case a different *E.coli* strain, BL21, was used. Upper mesh represents the 1st and bottom mesh the 2nd passage. Values at 0 MPa indicates cell suspension before homogenization.

pellet to compressed cell debris after homogenization, understandably at the same parameters. Table 3.2 shows the measured and calculated values.

Table 3.2.: Recovery rate at the disc stack centrifuge at different cell dry weight

	Paramters	Values				
Cell suspension	CDW [$\frac{g}{L}$]	25	40	50	60	94
	Solid fraction [%]	11	23.5	30	34	50
After homogenization	Solid fraction [%]	2.9	4	11	15.5	27
	Reduction factor [ ]	3.8	5.9	2.7	2.2	1.9
	C_{GFP} [$\frac{g}{L}$]	2.5	4.0	5.0	6.0	9.4
Centrifugation performance	No. of discharges	12	10	22	26	29
	Recovery rate [%]	**99**	**98**	**95**	**92**	**87**

An increased cell density resulted in a decrease of the reduction factor. This led to a higher number of discharges and to a reduced recovery rate.
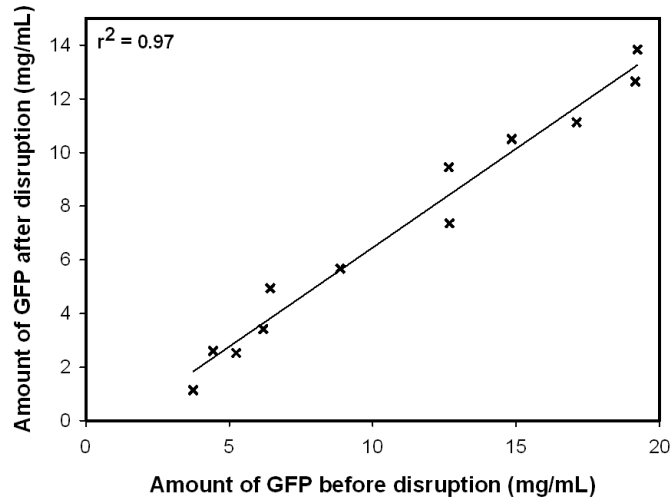
Figure 3.5.: Protein release at assumed 100% disrupted fraction as a function of amount of GFP determined through direct measurements of the cell suspension before homogenization. Correlation factor and trend line are shown in the plot. Fluorescence calibration was done with purified *GFP*.

3.2.4. Fluorescence measurements of cell suspensions and homogenates

Direct measurements of the cell suspension should provide a measure of the amount of soluble and intact GFP which is inside the cells. It was assumed that those values must be lower, caused by quenching effects. However, it turned out that these values were a lot higher for the HMS strain.

Fluorescence calibration curve was established with purified *GFP*. The fluorescence factor is 27693 $\frac{RFU}{\frac{mg}{mL}}$ (System specs see 2.3).

Figure 3.5 shows the correlation of measured *GFP* concentration of the cell suspension versus measured *GFP* concentration after homogenization. The function of the trend line is shown in equation 3.5.

$$y = 0.74 * x - 0.92 \tag{3.5}$$

Following possibilities might explain this effect:

- Not all protein is released. This could be ruled out. Because, as it was shown in previous data, at 90 MPa almost all protein is released.
- The redox potential inside the cell is different, resulting in a stronger fluorescence. It was not able to confirm this effect with a different strain (BL21).
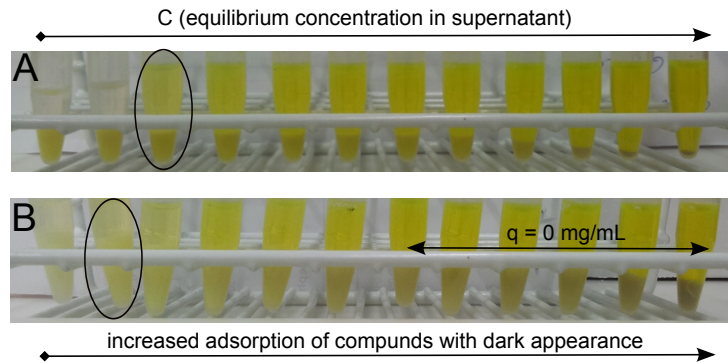
Figure 3.6.: Picture of an experimental set up of an adsorption isotherm of Q-Sepharosse FF after incubation with A) a diafiltrated and B) the cleared *E.coli* homogenate. Circle indicates the tube with the highest binding capacity. From right to left: With increasing feed concentrations, from 0.01 to 8 $\frac{mg}{mL}$ (A) and 0.4 to 10 $\frac{mg}{mL}$ (B), an adsorption of compounds with dark appearance are evident.

- Released GFP binds on the cell wall debris and, eventually, getting lost after centrifugation. According to Pekker.M and Shneider (2014) *E. coli* surface net charged is negative, as well as the net charge of GFP. Furthermore if this occurs due to an ionic bond, the homogenization buffer (0.1 mM NaCl) should minimize this effect.
- Possibly, the signal gets amplified by other cell wall proteins or even by itself caused by its tight packing.
- Inclusion bodies are fluorescing as well. This could be possible, because the folding process and establishing the fluorophore of the molecule are separated processes. Even though, the chromophore formation is the limiting step. However, it was seen that in solutions with dissolved inclusion bodies no adsorption at 485 nm was visible.

3.3. Anion exchange chromatography with a crude E.coli homogenates

3.3.1. Adsorption isotherm

Small scale batch adsorption tests are a useful tool to determine the kinetics of adsorption and the equilibrium capacity of a resin. In this work, two resins were characterized with different feed stocks. In figure 3.6 a picture of such a test is shown.
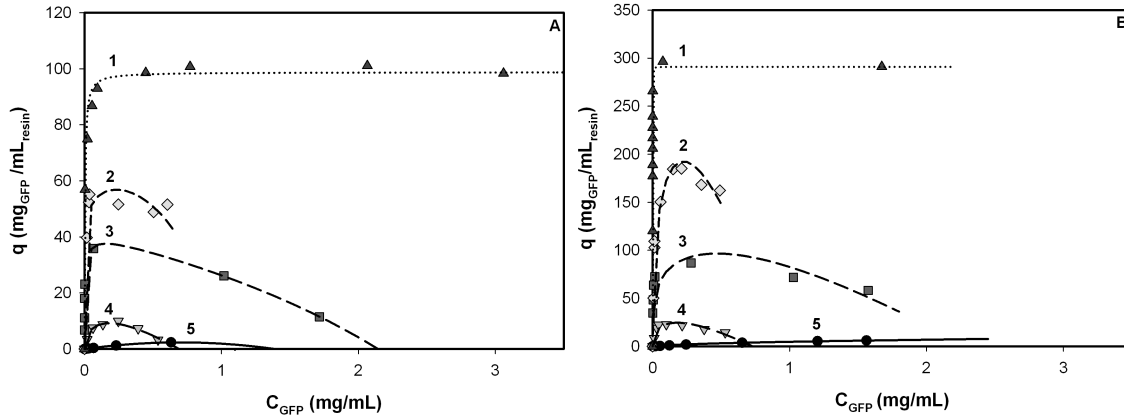
Figure 3.7.: Adsorptionisotherm of different feed stocks with A) Q-Sepharose FF and B) CaptoQ resin. 1) Pure GFP, 2) diluted diafiltrate, 3) diafiltrate, 4) diluted homogenate, 5) homogenate. Samples were diluted with water.

Both tests were realized with the resin Q Sepharose-FF, the incubation time was 24 h. In the first picture the resin was incubated with 0.2 μm filtrated homogenate. The second was performed with the same homogenate, previously diafiltrated with 7.5 volume changes of a salt less buffer. The homogenization had been performed at a cell density of 50 $\frac{g}{L}$ and a pressure of 90 MPa.

The batch experiment was done over a wide range of supernatant concentrations. This was realized by changing the volume of the resin added to the homogenate sample (calculation according to equation 2.1 and 2.2). In other words, the ratio of $\frac{GFP}{mL_{resin}}$ varied at each tube. It is clearly evident that with higher ratio the resin got darker. This happened at both test runs, even though at a lower ratio and more intense with the crude homogenate. Evidently, GFP was getting replaced at higher concentration.

Figure 3.7 shows a comparison of isotherms with different feed stocks. Here, the same effect is evident. At higher supernatant concentrations the binding capacity approached or rather was 0 $\frac{mg_{GFP}}{mL_{resin}}$. In contrast, pure GFP showed a common adsorption behavior without a displacement effect. This suggested that impurities were accountable for the displacement. As assumed the homogenate exhibited the lowest capacity. Diafiltrating enhanced the binding properties, due to the reduction of salt. Diluting the solutions with water had a positive effect on the isotherms, caused by the reduction of the ionic strength and impurity concentration of the samples.

Although different binding capacities were obtained both resins revealed the same displacement effect. CaptoQ bound much more protein than Q-Sepharose FF, due to its dextran surface extender.
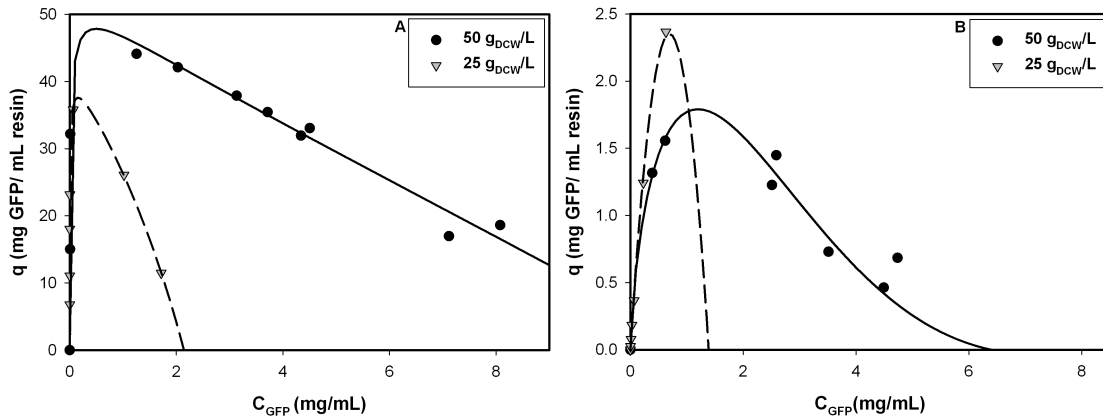
Figure 3.8.: Adsorptionsisotherm with Q-Sepharose FF of diafiltrated (A) and a crude homogenate (B). Disruption took place at different cell densities.

Furthermore, more than 5 volume changes in the diafiltration step didn't increase the level of the maximum binding capacity, neither was a delay in the decrease visible.

One noteworthy effect need to be mentioned. For a high cell density homogenate the binding capacity was enhanced (see figure 3.8). In this case precipitation events took place, but it cannot be confirmed that this was the reason for the better capacity.

Precipitation was dependent on the adjusted cell density for the homogenization step. It is concluded that the solubility limit of the impurities was reached. After precipitation, the solution exhibited lowered NTU values. This led to a higher capacity and to a decay in the decrease when approaching higher concentrations.

According to the empirical results following assumptions were made:

- The higher the feed concentration the lower the capacity
- CaptoQ revealed a higher binding capacity due to its surface extenders
- Diafiltrated homogenate exhibited a higher binding capacity

3.3.2. An example for modelling a two component adsorption isotherm

With the extended Langmuir Isotherm model (see equation 1.14 and 1.15) a two component adsorption process is comprehensible. Therefore a program was written in Python 2.7 (see appendix A). If both components parameters are known, which have been determined from a single component adsorption test, a full competitive

Table 3.3.: Adsorption isotherm parameters according to Garke et al. (1999)

Protein	$K_a[\frac{mL}{mol}]$	$q_m[\frac{mg}{mL_{resin}}]$
Lysozyme	$3.4 * 10^5$	101
γ-globulin	$5.6 * 10^5$	74

adsorption can be calculated. Figure 3.9 shows the computed output of a two compo-nent adsorption isotherm of γ-globulin and lysozyme. This system was first modelled by Garke et al. (1999). These parameters (see table 3.3) were used as prove of concept for the newly written program. q_m represent the maximum binding capacity achieved in a batch adsorption test. K_a is the Langmuir paramters also derived from a single component adsorption test.

As it is shown in the plot (1), one component got completely displaced by the other one. If the variables were normalized the picture is a little different.

At the second plot (2) θ_i, which represents the ratio of occupied to unoccupied sites on the resin, is shown as a function of the normalized concentration in the supernatant of γ-globulin. Here, it seemed that both components behave independently from each other up to a certain point. At that, γ-globulin was displaced when the feed concentration was increased.

If the results are plotted as a function of normalized feed concentrations of lysozyme (3), then it is evident that the displaced component was only present at very low feed concentrations of lysozyme. γ-globulin was only influencing at very low concen-trations which resulted in a slight reduction of the amount of adsorbed protein per increased feed concentration of lysozyme. Overall the adsorption of the component was negligible small influenced by the second one.

The last plot (4) describes the adsorption behavior of both proteins on the resin. In this case at every part of the adsorption isotherm lysozyme dominated the adsorption. The arrow indicates where the displacement happened. At this point up to 75 % of the accessible sites of the resin were occupied by the proteins.

For the shape of the competitive multicomponent adsorption the mass fraction was crucial. Garke et al. (1999) stated that due to its molecule size, the binding capacity of lysozym (14.1 kDa, pI = 11) was nearly unaffected by γ-globulin (156 kDA, pI = 6.5). The first one was smaller in size and shape. Therefore more binding sites were available. Furthermore, in this process lysozyme was more charged than the other protein, which results in a higher attraction to the resin, indicated by the different slopes of isotherms.
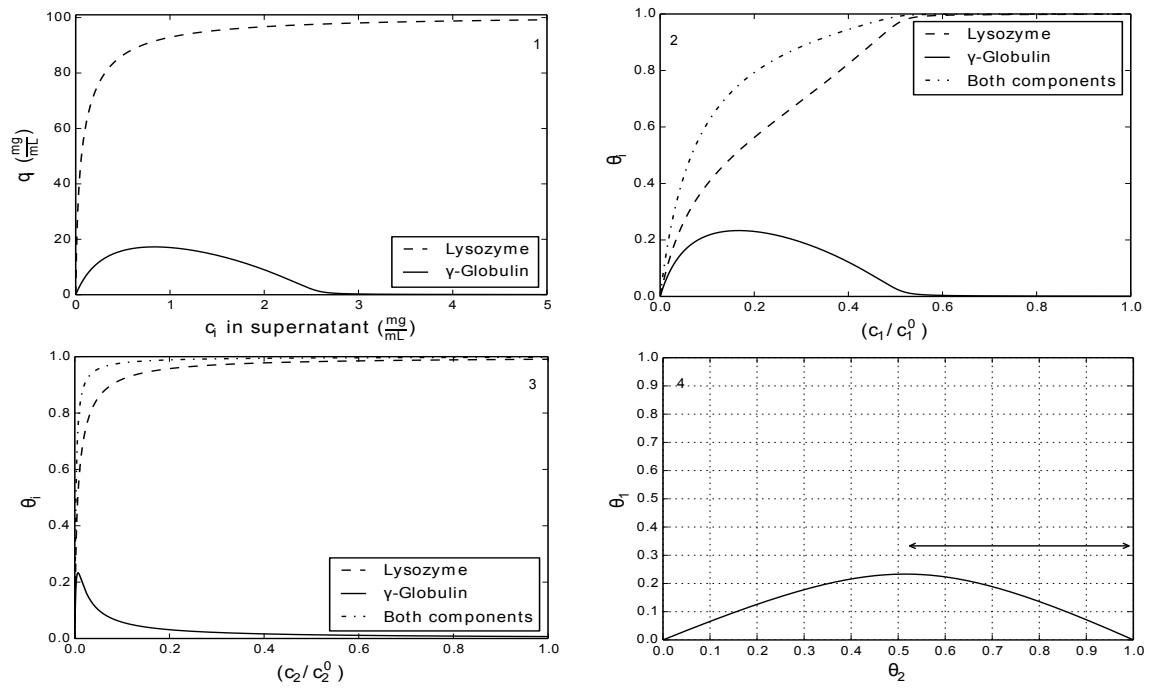
Figure 3.9.: Model of a two component adsorption system of γ-globulin and lysozyme. Mass fraction of γ-globulin and lysozyme = 1:3. Used parameters according to Garke et al. (1999). 1) Binding capacities of both components as a function of their feed concentrations. 2) Fractional occupancy of both as a function of the normalized feed concentrations of γ-globulin. 3) Fractional occupancy of both as a function of the normalized feed concentration of lysozyme. 4) θ_1 (γ-globulin) as a function of θ_2 (lysozyme). Arrow indicates the displacement effect.
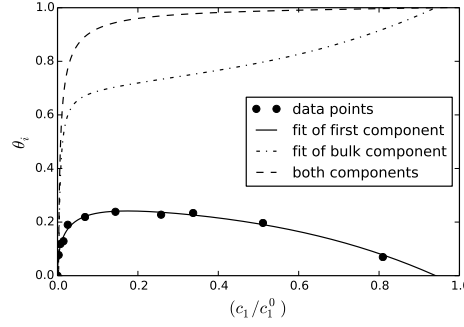
Figure 3.10.: Fitting of a assumed second bulk component out of an adsorption isotherm from a diafiltrated *E.coli* homogenate.

According to the above mentioned results, four obvious possibilities can be carried out, how two proteins will behave on an ion exchange resin under binding conditions. It is assumed that, specific parameters like buffer composition, pH, salt content and the most important one, the mass fraction of both components will stay constant and multi-layer adsorption or excessive hindrance are not taken into account:

ΔpI represents the difference of the isoelectric points of component 2 to 1. Δd is referred to the protein size difference of component 2 to 1, which can also be expressed as an approximation of the molecular weight in kDa.

- If $\Delta pI > 0$ and $\Delta d > 0$ is true, component 1 will be displaced by component 2.
- If $\Delta pI > 0$ and $\Delta d \sim 0$ is true, binding capacity will decrease for each protein. The displacement effect will occur, to a minor extent.
- If $\Delta pI \sim 0$ and $\Delta d > 0$ is true, component 1 will bind less favourable. In a minor way, the displacement effect will occur.
- If $\Delta pI \sim 0$ and $\Delta d \sim 0$ is true, no displacement should occur.

Point 1 and 2 was proven by Garke et al. (1999) and by Liang et al. (2012), respectively.

Whereas case 1 will result in a displacement, the other three ones will just reduce the maximum binding capacity with a possibility of a slight displacement at higher feed concentrations.

If the replaced component is known, q_{max} and K_a, respectively, the second one is also determined. With normalizing the feed concentration and using the fractional occupancy θ, it was possible to calculate the normalized binding occupancy as a function of the normalized feed concentration of the displaced component (see figure 3.10). Only at very low concentrations ($x \to 0$) the deviation was a little increasing, which was contributed to the mathematical model.

Figure 3.11.: Binding capacity as a function of time at two different feed concentrations of *E.coli* homogenate with a A) Q-Sepharose FF and B) CaptoQ resin. Homogenization was performed with a cell density of 25 $\frac{g_{DCW}}{L}$

However, in bioprocess operation are far more unknown components present, like it is the case in a *E. coli* homogenate. Therefore, it was assumed that the impurities, which contributed to the displacement effect, could be summed up to one bulk component. This one had to be smaller in size and a higher pI as GFP. If components are present which were replaced by GFP itself, they were only having an impact at very low feed concentrations and could be neglected. All other components had only a negligible effect on the isotherm.

3.3.3. Kinetics of multicomponent adsorption

In the section 3.3.1 and 3.3.2 displacement effects were considered only for the equilibrium situation. Complete validation of such a replacement of proteins requires also a consideration of kinetics.

Therefore, kinetic batch tests were performed to determine the protein uptake rates. It was done for a purified GFP, a diafiltrate and a clarified *E. coli* homogenate at different feed concentrations with the resins CaptoQ and Q-Sepharose FF, respectively.

Figure 3.11 shows adsorption kinetics at two different feed concentrations on Q-Sepharose FF and CaptoQ. It is clearly evident that for both resins at higher concentrations an overshoot above equilibrium took place, which was approaching zero at a longer process time. The overshoot were lesser pronounced at lower concentrations. Both resins were revealing almost the same shape, only differed in the absolute values. CaptoQ bound much more protein due to its surface extender. This could also be
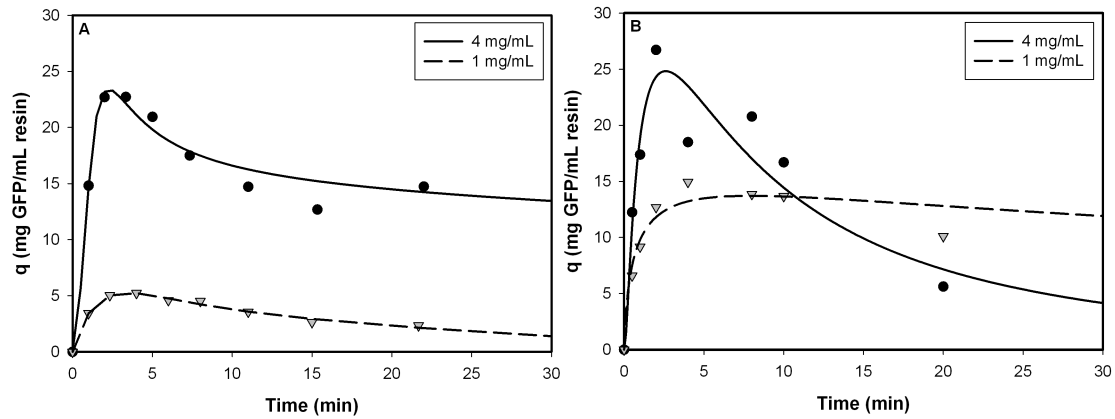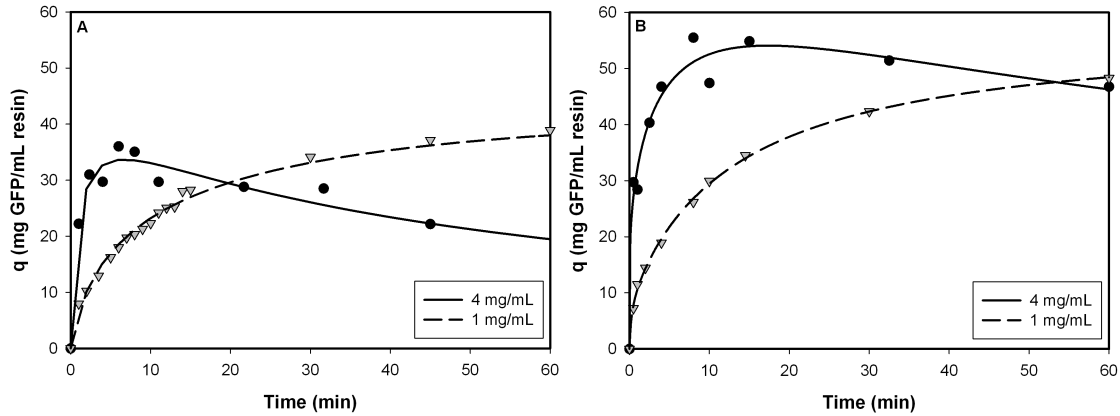
Figure 3.12.: Binding capacity as a function of time at two different feed concentrations of a diafiltrated *E. coli* homogenate on a Q-Sepharose FF resin. Processing A) before and B) after precipitation emerged.

the reason, why the binding capacity of CaptoQ was much faster decreasing at high feed concentration. Possibly, due to the extender the dominant impurities had easier access to the occupied binding sites.

The same displacement effect was evident with a diafiltrated *E. coli* homogenate (see figure 3.12). The overall binding capacity was higher and also at higher feed concentrations an overshoot above equilibrium was existent.

Comparing the results a remarkably difference in the binding capacity can be seen. After separating the cell debris, some precipitation occurred. Plot A shows a low, and B a high cell density homogenate. In the latter one a high amount of precipitate occurred after a short period of time. It was removed by centrifugation and exhibited, as it is shown in the plot, a higher binding capacity. Accordingly, this suspension exhibited a lesser impurity level.

At a lower cell density homogenate some precipitation also occurred, but not in that manner.

Purified GFP (see figure 3.13) exhibited no displacement behaviour.

Table 3.4 shows the maxima of the binding capacities and the time when they appeared.

It is evident that the overshoot above equilibrium was most pronounced at high feed concentrations. The higher it was, the faster q was approaching zero with ongoing time. Additionally, the maximum of the peak was at earlier times when the feed concentration was high. Remarkably, the diafiltrated homogenate, in comparison with
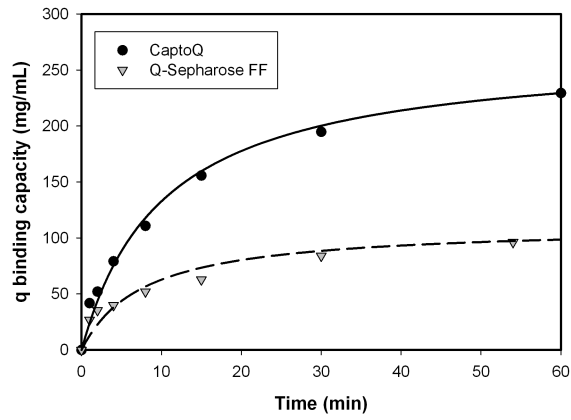
Figure 3.13.: Binding capacity of a purified GFP as a function of time on Q-Sepharose FF and CaptoQ.

the non-ones, exhibited its maximum binding capacity at a later point at the same feed concentrations.

However, it appears that the impurity level revealed somehow a higher driving force, which resulted in a faster binding- and displacement rate of GFP.

The displacement kinetic can be described by the shrinking core model. Here, GFP approaches the center of the particle during incubation. GFP is displaced by the second component at the outer region of the resin fragment. After a certain time the impurities are fully occupying the binding sites.

Table 3.4.: Maxima of the binding capacities and the time when they appear of each adsorption kinetics experiment

Resin	Sample	homogenated cell density $[\frac{g_{DCW}}{L}]$	Feed concentration $[\frac{g}{L}]$	Maxima $[\frac{mg_{GFP}}{mL_{resin}}]$	Time [min]
Q-Sepharose FF	Homogenate	≈ 25	4.1	21.6	2.1
			1.2	5.3	3.4
		≈ 50	7.1	37.2	1.6
			3.7	8.3	2.3
			0.9	3.4	9.5
	Diafiltrate	≈ 25	4.8	33.9	5.9
			0.9	41.3	179.7
		≈ 50	6.8	38.7	11.2
			3.8	54.1	17.3
			1.1	>50	>60
	pure GFP	-	0.4	111.2	>140
CaptoQ	Homogenate	≈ 25	4.0	24.8	2.6
			1.2	13.7	7.9
	Diafiltrate	≈ 25	4.4	86.6	23.5
	pure GFP	-	0.4	268.5	>140
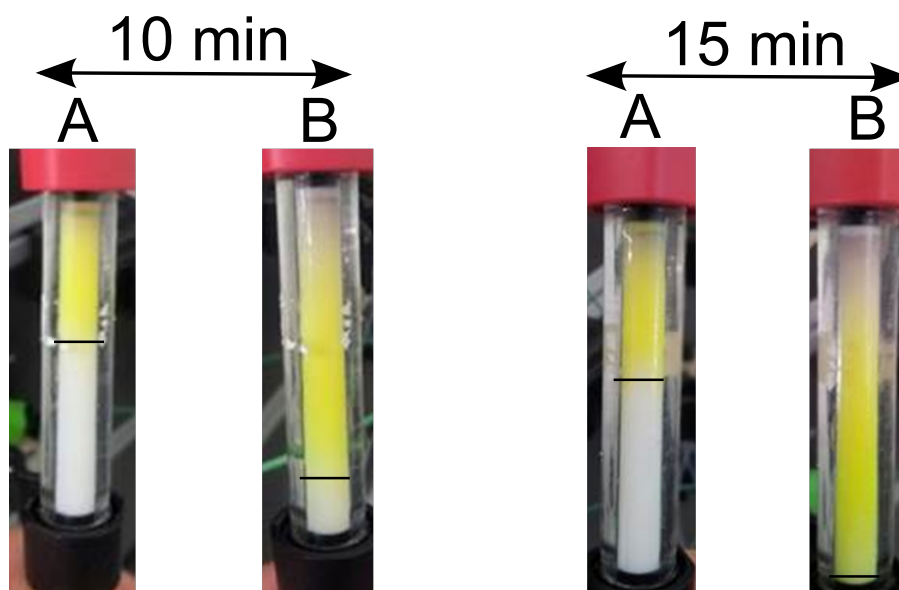
Figure 3.14.: Pictures of the occurring displacement effect in a 1 mL Q-Sepharose FF Tricorn column at different residence times (10 min and 15 min, respectivley). The yellowish area represents the location of the GFP in the column. The remaining white area is unoccupied resin. Horizontal line indicates the front of the GFP. A) After loading of GFP is completed. B) After wash out phase, with 2 CV, is completed.

3.3.4. Multicomponent behavior in the column

Figure 3.14 shows pictures of a Tricorn column packed with 1 mL of a Q-Sepharose FF. The left side represents the column after loading *E. coli* homogenate with a feed concentrations of $4 \frac{mg}{mL}$ and the right side after the wash out phase (2 CV). This experiments were done at two different residence times, 15 min and 10 min, respectively. During the wash out step the GFP front, which is indicated by the solid line, was travelling further down in the column. The upper region became more ore less devoid of protein, revealing a dark greyish product concentrated in a few millimeters. This impurity was also seen at the adsorption isotherm and kinetic experiments.

The results shown above, assumes a specific behavior when the sample is loaded on the column. At high feed concentration a short residence time seems to be ideal. In contrast, at low feed concentrations a slower flow rate at the loading step is needed to reach a high binding capacity.

To estimate the dynamic binding capacity break through curves were performed. As it was discussed in the section 1.6 preparative chromatography only depends on diffusional properties. Low flow rates and high feed concentrations are positively
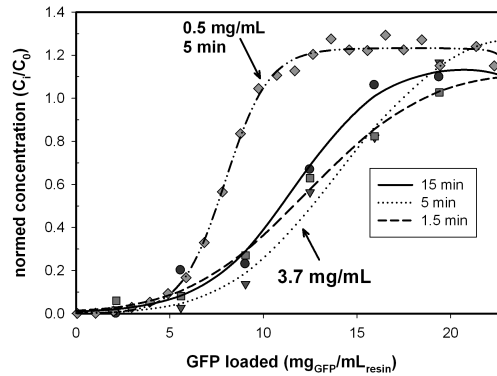
Figure 3.15.: Break through curves at different residence times and feed concentrations on a Q-Sepharose FF resin. The low feed concentrations is separately indicated by the arrow.
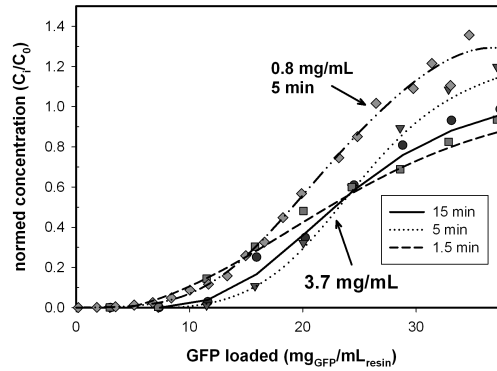
Figure 3.16.: Break through curves at different residence times and feed concentrations on a CaptoQ resin. The low feed concentrations are separately indicated by the arrow.

affecting pore diffusion and will lead to a higher dynamic binding capacity (DBC) Figure 3.15 shows that with a higher feed concentrations a greater DBC was reached. Additionally, an overshoot above the normalized concentration is visible ($\frac{c_i}{c_0} > 1$), which is a result of the displacement effect.

Remarkably, the DBC was independent on the used residence time. By comparing figure 3.15 with figure 1.11 it is obvious that the binding capacity should behave differently if only pore diffusion is taken into account.

The effect was the same for the resin CaptoQ (see figure 3.16). Although this resin was not as sensitive as Q-Sepharose FF to a varying residence time (see figure 1.10), the shift in the BTC's were quite distinctive. i.e., at a residence time of 5 min and a feed concentration of 3.7 $\frac{mg}{mL}$ the highest dynamic binding capacity was reached.

46
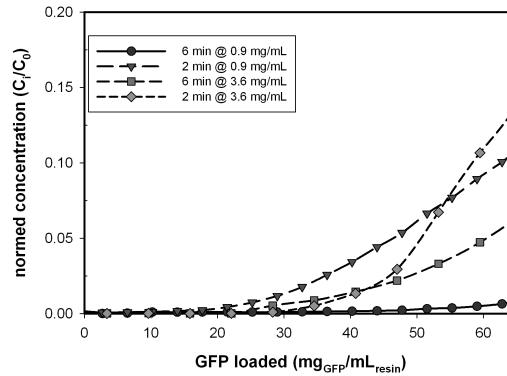
Figure 3.17.: Break through curves with a diafiltrated *E. coli* homogenate at different residence times and feed concentrations on a Q-Sepharose FF resin.
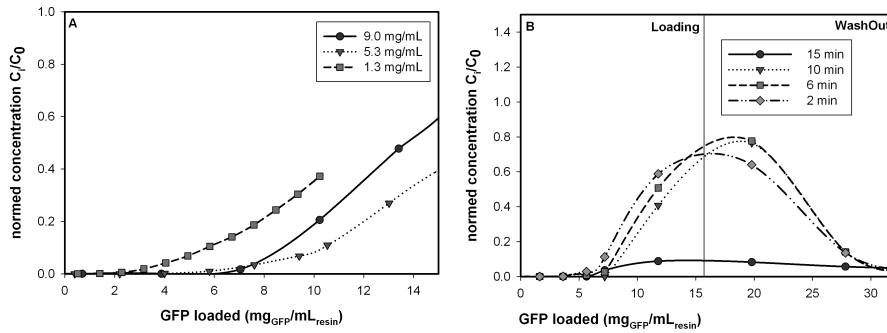
Figure 3.18.: Break through and wash out behaviour of a *E.coli* homogenate on a Q-Sepharose FF resin. A) BTC's at different feed concentrations at a residence time of 6 min. B) BTC's at different residence time with a feed concentration of $9.0 \frac{mg}{mL}$. Vertical line indicates the end of the loading step.

Figure 3.17 shows a break through curves at different residence times and feed concentrations on a Q-Sepharose FF resin. In case of the diafiltrated *E. coli* homogenate, pore diffusion became the more dominant effect. Contrary to the homogenate BTC's, at a higher residence time a greater dynamic binding capacity was reached. Furthermore, when lowering the feed concentrations a higher DBC was also achieved.

Figure 3.18 shows again the behavior of the break through curve at changes in the feed concentrations at a specific residence time. The wash out phase after loading is shown in plot B.

The first plot (A) shows the above discussed behavior at changing feed concentrations. Astonishing, at a certain point the DBC again decreased. This was a result of the

above seen kinetic behavior. The higher the feed concentration was the higher was the overshoot above equilibrium but also the faster is the decrease approached to 0.

The latter plot shows the loading and the wash out phase (indicated by the vertical solid line) during chromatography. The displacement is not finished with the loading step. It washed out some of the loaded product, resulting in a lowered recovery.

Remarkably was that a very high residence time (15 min) the binding capacity increased dramatically and no or at least a little wash out was evident. This seems to be the other extreme of this displacement effect.

To understand this behavior the column should be separated into different zones. In the first one GFP gets displaced in the upper region of the column (1st zone) and the impurities bind completely. When the product enters the second one the capacity of GFP is increased. Here, little rest of the interfering particles but also the main products bind. Displacement occurs only to a minor extent. In the last zone only GFP is bound. Under specific conditions (high feed concentration and high residence time), the impurities are completely adsorbed in the 1st zone, resulting in an enhanced binding capacity of GFP and a minor wash out.

The mechanism of the displacement leads to a deceptive illustration of the dynamic binding capacity. This discrepancy is dependent on following process characteristics:

- Cell density at the homogenization step
- Diafiltrating
- Loaded amount of GFP
- Feed concentration
- Residence time

These entire variables are influencing the DBC. If you going into more detail, much more parameters must be added, i.e. fermentation characteristics. Accordingly, comparing different chromatography runs were kind of difficult. At least two parameters had to stay constant to be able to draw comparisons.

Figure 3.19 shows the recovery of a *E. coli* homogenate as a function of residence time and feed concentration. The loaded amount of GFP was 15 $\frac{mg_{GFP}}{mL_{resin}}$ and the used cell density for the homogenization progress was 50 $\frac{g_{DCW}}{L}$. The recovery was estimated according to the simple equation 3.6. In this case it is evident that at higher feed concentrations the recovery decreased. It is also shown that the recovery was nearly unaffected by the residence time. But at a certain point the behavior was changing. As discussed above at high feed concentrations and residence time the impurities with a very high binding capacity bound completely in the upper region of the column. Resulting in a higher binding capacity of GFP in the next region of the column. This is due to the fact that the displacement effect is a time dependent phenomenon.
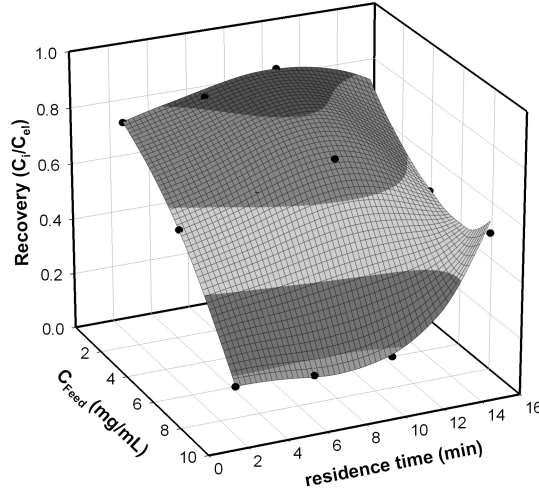
Figure 3.19.: Recovery as a function of residence time and feed concentration. Used sample was a *E.coli* homogenate and used resin was Q-Sepharose FF. Around 15 $\frac{mg_{GFP}}{mL_{resin}}$ had been loaded. Cell density at the homogenization process was 50 $\frac{DCW}{L}$.

$$Recovery \; \frac{m^{GFP}_{Eluate}}{m^{GFP}_{Load}} = \frac{Amount \; of \; GFP \; in \; eluate}{C_i V_{load} - Amount \; of \; GFP \; lost \; during \; the \; loading \; step} \qquad (3.6)$$

Figure 3.20 shows a simplistic proposed mechanism of the displacement effect for a diafiltrated *E.coli* homogenate in the column. For that purpose, all ordinates are normalized. t_0 represents the time at which the binding capacity q_i approaches zero at the beginning of the column. $q_{i;max}$ is the maximum binding capacity which can be achieved at every step i $\{i \in \mathbb{R} | i > 0\}$. Here, it is important to mention that $q_{i;max} \neq q_{max}$. The discussed model is only valid within specific constraints. The displacement effect must happen in a short period of time and as a simultaneous multicomponent adsorption. The maximum binding capacity for the impurities is a lot higher than that from GFP. Differences in the supernatant concentration, as a result of desorption processes, are negligible small. Also radial diffusion is not taken into account. In this thought experiment a short pulse with a crude homogenate is applied onto the column.

In this plot the displacement effect is pretty clear at the beginning of the column. In the first region GFP gets completely displaced. Here, the maximum of the binding capacity is at a earlier point of time. The impurities will get mostly bound in the first region due to their high binding capacity.
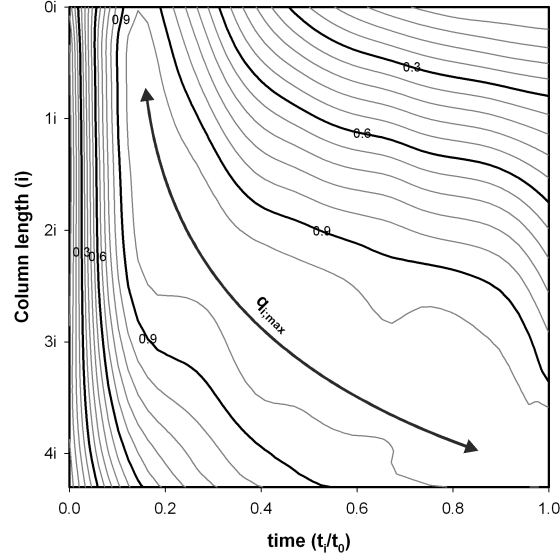
Figure 3.20.: Obtainable binding capacity as a function of time and column length. t_0 is stated as the time where complete displacement at column length $\to 0i$ occured. Arrow indicates the area where 100 % binding capacity is reached $\{0 \le q_{i;max} \ge 1\}$.

With ongoing progress the concentration of the impurities is greatly depleted thus, results in a lesser displacement. Due to the fact that GFP is also binding the concentration of it is decreasing along the column length. More time is now needed to achieve the maximum binding capacity.

This proposed mechanism is truly consistent with the above discussed results (i.e. see figure 3.14) and the mentioned theory (see 1.6.4). For establishing a complete mathematical model much more work needed to be done, but G. Carta et al. (2005) and Traylor et al. (2011) did a good job on that point. The influence of many variables make a quantitative prediction of the behavior quite difficult and more data is needed to reduce the discrepancies to a minimum.

4. Conclusion

Purification of recombinant GFP produced in *E. coli* was chosen as a model process for elucidating homogenization and anion exchange chromatography. *E. coli* is a widely used organism in industry, while the stable fluorescence properties of GFP permit easy validation for the unit operations.

During homogenization, protein yield was not influenced by the used cell density. The efficiency of the process was strongly correlated to the used operational pressure.

Furthermore, a correlation between the viscosity and the correspondent solid volume was established. This tool provides a fast method for determination of the pellet volume from cell suspensions and homogenates respectively.

Another important part in this master thesis was to elucidate the multicomponent adsorption on anion exchange resins of a diafiltrated and a crude homogenate.

The best chromatographic performance was achieved with a diafiltrated *E. coli* homogenate. Under this conditions, kinetic batch test showed that a weaker and delayed displacement of GFP occurred. Furthermore, highest dynamic binding capacity was observed at low feed concentrations and high residence times. The recovery rates were always above 90%.

In contrast, for the crude homogenate kinetic data suggested a high binding capacity at a short residence time and high feed concentrations. However, the recovery of GFP in eluate was quite low. A high amount of protein was lost during the wash out phase.

Below future work is described which can be important for the homogenization process.

Obviously, the size of the cell debris is dependent on the pressure and the number of passages. A relationship of turbidity of the solution and the averaged particle diameter was observed. Establishing a correlation between them can help to improve the subsequent filtration process.

Although the homogenization process has been investigated by many authors, no one has provided a simpler model to compare the homogenization efficiency between

different organism and strains. This can be an important instrument for screening applications.

Improvements in anion exchange chromatography process are described in the next paragraphs.

At high feed concentrations, especially with the crude homogenate, an increase of adsorbed impurities with a dark appearance occurred. Even the CIP procedure, using a 2 M NaCl and 0.25 M NaOH buffer, was not able to reduce this discoloration, suggesting irreversible bound impurities. A depleting binding capacity will occur over time. To avoid loss of chromatographic performance, a second column can be connected upstream. The function of the second column (the guard column) is to adsorb the dark appearing impurities and to reduce the displacement effect on the main column to a minimum. Due to the high binding capacity of those compounds a small amount of resin is sufficient. The main column must be appropriate in size for the capturing process. The method can be performed as follows:

Crude homogenate is applied onto the guard column. A high feed concentration and a low residence time is recommended to ensure a complete displacement of GFP. The flow through is collected and subsequently applied onto the main column. The advantages would be:

- No loss of protein of interest in the wash out phase of the main column, which will result in a high recovery rate.
- Enhanced durability of the main column
- Reduction of process time and costs by bypassing the diafiltration step.
- Reduction of process volume, time and costs due to the requirement of high product titer.

Characterization of the second component will be another important step in future. This can help to reduce the amount of interferring impurities in advance by adjusting process paramters or even by developing new mutants of *E. coli*.

Bibliography

Balasundaram, Bangaru, Sue Harrison, and Daniel G. Bracewell (2009). "Advances in product release strategies and impact on bioprocess design." eng. In: *Trends in biotechnology* 27 (8). Journal Article Research Support, Non-U.S. Gov't Review, pp. 477–485. ISSN: 1879-3096. DOI: 10.1016/j.tibtech.2009.04.004. eprint: 19573944 (cit. on p. 11).

Broughton, D. B. (1948). "Adsorption Isotherms for Binary Gas Mixtures." In: *Industrial and engineering chemistry* 40 (8), pp. 1506–1508 (cit. on p. 17).

Carta, G., a. R. Ubiera, and T. M. Pabst (2005). "Protein Mass Transfer Kinetics in Ion Exchange Media: Measurements and Interpretations." In: *Chemical Engineering & Technology* 28 (11), pp. 1252–1264. ISSN: 0930-7516. DOI: 10.1002/ceat.200500122 (cit. on pp. 13, 18, 19, 50).

Carta, Giorgio (2012). "Predicting protein dynamic binding capacity from batch adsorption tests." eng. In: *Biotechnology journal* 7 (10). Journal Article Review, pp. 1216–1220. ISSN: 1860-7314. DOI: 10.1002/biot.201100475. eprint: 22745056 (cit. on p. 15).

Carta, Gorgio and Alois Jungbauer (2010). *Protein Chromatography. Process Development and Scale-Up*. WILEY-VCH Verlag. ISBN: 978-3-527-31819-3 (cit. on pp. 12, 13, 15).

Chalfie, Martin, Y. Tu, G. Euskirchen, W. W. Ward, and D. C. Prasher (1994). "Green fluorescent protein as a marker for gene expression." In: *Science* 263 (5148). February, pp. 802–805. DOI: 10.1126/science.8303295 (cit. on p. 1).

Clarke, A., T. Prescott, A. Khan, and A. G. Olabi (2010). "Causes of breakage and disruption in a homogeniser." In: *Applied Energy* 87 (12), pp. 3680–3690. ISSN: 03062619. DOI: 10.1016/j.apenergy.2010.05.007 (cit. on pp. 9, 10).

Doran, Pauline M. (2012). *Bioprocess Engineering Principles. Second Edition*. Academic Press. ISBN: 978-0-12-220851-5 (cit. on p. 7).

Flickinger, Michael C., ed. (2013). *Downstream Indsutrial Biotechnology. Recovery and Purification*. ISBN: 978-1-118-13124-4 (cit. on p. 9).

Garke, G., R. Hartmann, N. Papamichael, W.-D. Deckwer, and F. B. Anspach (1999). "The Influence of Protein Size on Adsorption Kinetics and Equilibria in Ion-Exchange Chromatography." In: *Separation Science and Technology* 34 (13), pp. 2521–2538. ISSN: 0149-6395. DOI: 10.1081/SS-100100788 (cit. on pp. 18, 38–40).

GE Healthcare Life Sciences (2014a). "Data file 18-1177-22 AE. Sepharose Fast Flow ion exchange media and prepacked column formats." In: (cit. on p. 12).

GE Healthcare Life Sciences (2014b). "Datafile 11-0025-76 AG. Capto S, Capto Q, Capto DEAE." In: (cit. on p. 12).

Gu, Tingyue, Gow-Jen Tsai, and George T. Tsao (1991). "Multicomponent Adsorption and Chromatography with Uneven Saturation Capacities." In: *AlChE Jorunal* 37 (9), p. 1333 1340 (cit. on p. 17).

Hahn, Rainer (2012). "Methods for characterization of biochromatography media." eng. In: *Journal of separation science* 35 (22). Journal Article Research Support, Non-U.S. Gov't Review, pp. 3001–3032. ISSN: 1615-9314. DOI: 10.1002/jssc.201200770. eprint: 23111926 (cit. on pp. 13–15).

Hashim, M. A. and K. H. Chu (2007). "Prediction of protein breakthrough behavior using simplified analytical solutions." In: *Separation and Purification Technology* 53 (2), pp. 189–197. ISSN: 13835866. DOI: 10.1016/j.seppur.2006.06.028 (cit. on p. 14).

Heim, Roger, Douglas C. Prashert, and Roger Y. Tsien (1994). "Wavelength mutations and posttranslational autoxidation of green fluorescent protein." In: *Proceedings of the National Academy of Sciences of the United States of America* 91 (December), pp. 12501–12504 (cit. on pp. 2, 3).

Jungbauer, Alois (1996). "Insights into the chromatography of proteins provided by mathematical modeling." In: *Current Opinion in Biotechnology* 7 (2), pp. 210–218. ISSN: 09581669. DOI: 10.1016/S0958-1669(96)80015-2 (cit. on p. 13).

Letki, A. G. (2000). "CENTRIFUGATION — Theory of Centrifugation." In: *Encyclopedia of Separation Science*. Elsevier, pp. 336–342. ISBN: 9780122267703. DOI: 10.1016/B0-12-226770-2/04631-7 (cit. on p. 8).

Liang, Juan, Georg Fieg, Qing-hong Shi, and Yan Sun (2012). "Single and binary adsorption of proteins on ion-exchange adsorbent: The effectiveness of isothermal models." eng. In: *Journal of separation science* 35 (17). Evaluation Studies Journal Article Research Support, Non-U.S. Gov't, pp. 2162–2173. ISSN: 1615-9314. DOI: 10.1002/jssc.201200101. eprint: 22888059 (cit. on p. 40).

Mergulhão, F J M, D. K. Summers, and G. A. Monteiro (2005). "Recombinant protein secretion in Escherichia coli." eng. In: *Biotechnology advances* 23 (3). Journal Article Review, pp. 177–202. ISSN: 0734-9750. DOI: 10.1016/j.biotechadv.2004.11.003. eprint: 15763404 (cit. on p. 6).

Morin, James G. and John Woodland Hastings (1971). "Energy transfer in a bioluminescent system." In: *Journal of Cellular Physiology* 77, pp. 313–318. DOI: 10.1002/jcp.1040770305 (cit. on p. 1).

Novagen (2003). "pET System Manual." In: (TB055 10th edition Rev.B 0403) (cit. on pp. 5, 6).

Overton, Tim W. (2014). "Recombinant protein production in bacterial hosts." eng. In: *Drug discovery today* 19 (5). Journal Article, pp. 590–601. ISSN: 1878-5832. DOI: 10.1016/j.drudis.2013.11.008. eprint: 24246684 (cit. on pp. 4, 5).

Bibliography

Pekker.M and M. N. Shneider (2014). *The surface charge of a cell lipid membrane*. Ed. by Pekker.M. Cornell University Library. URL: http://arxiv.org/abs/1401.4707v2 (visited on 04/07/2015) (cit. on p. 35).

Reid, Brian G. and Gregory C. Flynn (1997). "Chromophore Formation in Green Fluorescent Protein." In: *Biochemistry* 97403 (97), pp. 6786–6791 (cit. on pp. 2, 3).

Sanders, Jeremy K M and Sophie E. Jackson (2009). "The discovery and development of the green fluorescent protein, GFP." In: *Chemical Society reviews* 38 (10). oct, PubMed ID: 19771328, pp. 2821–2822. ISSN: 1460-4744. DOI: 10.1039/b917331p. URL: http://www.ncbi.nlm.nih.gov/pubmed/20127319 (cit. on pp. 1, 2).

Sauer, Thomas, Campbell W. Robinson, and Bernhard R. Glick (1989). "Disruption of Native and Recombinant *Eschericha Coli* in a High-Pressure Homogenizer." In: *Biotechnology and Bioengineering* 33, pp. 1330–1342 (cit. on p. 10).

Shimomura, Osamu, Johnson Frank H., and Saiga Yo (1962). "Extraction, purification and properties of aequorin, a bioluminescent protein from the luminous hydromedusan, Aequorea." In: *Journal of Cellular and Comparative Physiology* 59 (3), pp. 223–239 (cit. on p. 1).

Shukla, Abhinav A. (2006). "Process Scale Bioseparations for the Biopharmaceutical Industry." In: (cit. on p. 9).

Skidmore, Graham L. and Howard A. Chase (1990). "Two-component protein adsorption to the cation exchanger S Sepharose FF." In: *Journal of Chromatography A* 505 (2), pp. 329–347. ISSN: 00219673. DOI: 10.1016/S0021-9673(01)93048-1 (cit. on p. 17).

Stone, Melani C. and Giorgio Carta (2007). "Patterns of protein adsorption in chromatographic particles visualized by optical microscopy." eng. In: *Journal of chromatography. A* 1160 (1-2). Journal Article Research Support, U.S. Gov't, Non-P.H.S., pp. 206–214. ISSN: 1873-3778. DOI: 10.1016/j.chroma.2007.05.058. eprint: 17560582 (cit. on pp. 15, 16).

Tóth, József (2003). "On thermodynamical inconsistency of isotherm equations: Gibbs's thermodynamics." In: *Journal of Colloid and Interface Science* 262 (1), pp. 25–31. ISSN: 00219797. DOI: 10.1016/S0021-9797(03)00236-4 (cit. on p. 15).

Traylor, Steven J., Xuankuo Xu, and Abraham M. Lenhoff (2011). "Shrinking-core modeling of binary chromatographic breakthrough." eng. In: *Journal of chromatography. A* 1218 (16). Journal Article Research Support, U.S. Gov't, Non-P.H.S., pp. 2222–2231. ISSN: 1873-3778. DOI: 10.1016/j.chroma.2011.02.020. eprint: 21411102 (cit. on pp. 18, 20, 50).

Tsien, Roger Y. (1998). "THE GREEN FLUORESCENT PROTEIN." In: *Annual Reviews of Biochemistry* (67), pp. 509–544 (cit. on pp. 1, 2, 4).

van Hee, Pim, Middelberg, Anton P J, Van Der Lans, Rob G J M, and Van Der Wielen, Luuk A M (2004). "Relation between cell disruption conditions, cell debris particle size, and inclusion body release." eng. In: *Biotechnology and Bioengineering* 88 (1). Comparative Study Journal Article Research Support, Non-U.S. Gov't, pp. 100–110. DOI: 10.1002/bit.20343. eprint: 15449302 (cit. on p. 11).

Bibliography

Wong, H. H., B. K. O'Neill, and A.P.J. Middelberg (1997). "A mathematical model for Escherichia coli debris size reduction during high pressure homogenisation based on grinding theory." In: *Chemical Engineering Science* 52 (17), pp. 2883–2890. ISSN: 00092509. DOI: 10.1016/S0009-2509(97)00105-X (cit. on p. 10).

Yang, Kun and Yan Sun (2007). "Structured parallel diffusion model for intraparticle mass transport of proteins to porous adsorbent." In: *Biochemical Engineering Journal* 37 (3), pp. 298–310. ISSN: 1369703X. DOI: 10.1016/j.bej.2007.05.011 (cit. on pp. 15, 16).

Appendix

Appendix A.

Python source code for the full competitve extendend Langmuir isotherm

```
    Multicomponent Isotherme by Sissolak B., August 2014


import numpy as np
from scipy import optimize
from matplotlib import pyplot as plt
%matplotlib inline

c_0 = np.zeros(2)
c_00 = np.zeros(2)
qm = np.zeros(2)
k = np.zeros(2)
mfc = np.zeros(2)

na = 'na'         # if no information is available or necessary
steps = 10000 #number of steps. for calculating
theta = np.array([np.zeros(2),steps])


Parameters

epsilon = 0    # particle porosity
qm1 = 74         # [mg/mL] maximum binding capacity component 1
qm2 = 101        # [mg/mL] maximum binding capacity component 2
Ka1 = 1/0.9   # [mL/mg] adsorptionconstant component 1
Ka2 = 1/0.041 # [mL/mg] adsorptionconstant component 2
names={1:r'$\gamma$-Globulin',2:'Lysozyme'} #put component's name
#with the highest qm on place2

c_01 = 5          # [mg/mL] component1 concentration at start
c_02 = na         # [mg/mL] component2 concentration at start
mfc1 = 0.2        # mass fraction component 1 from 0 to 1
mfc2 = na      # mass fraction component 2 from 0 to 1


If rules Part 1

# if rules below, ensure that the right way for further computing
#is choosen and calculates the rest of the missing variables
```

58

Appendix A. Python source code for the full competitve extendend Langmuir isotherm

```python
# for variables definition see 'Parameters'
# c_oo is a paramter wich helps to set the start concentrations in its right place (--> see
    next If rules).

if mfc1 is 0:
        print ('mfc1 = 0 --> single component Langmuir Isotherme')

elif mfc2 is 0:
        print ('mfc 2 = 0 --> single component Langmuir Isotherme')

elif c_02 is 'na' and mfc2 is 'na':
        print ('c_02 and mfc2 will be calculated ...')

        c_oo[0] = c_01
        mfc[0] = mfc1
        c_oo[1] = (c_01-c_01*mfc1)/mfc1
        mfc[1] = 1 - mfc[0]

elif c_01 is 'na' and mfc1 is 'na':
        print ('c_01 and mfc1 will be calculated ...')

        c_oo[1] = c_02
        mfc[1] = mfc2
        c_oo[0] = (c_02-c_02*mfc2)/mfc2
        mfc[0] = 1 - mfc[0]

elif mfc1 is 'na' and mfc2 is 'na':
        print('mfc1 and mfc2 will be calculated ...')

        c_oo[0] = c_01
        c_oo[1] = c_02
        mfc[0] = c_01/(c_01+c_02)
        mfc[1] = 1 - mfc[0]

elif c_01 is 'na' and c_02 is 'na':
        print ('calculating with mfc1/mfc2 = c1/c2')

        c_oo[0] = mfc1
        c_oo[1] = mfc2
else:
    print ('Please, check variables again!!!')

c_02 and mfc2 will be calculated ...


If rules part 2

# Its important to set the component with the highest binding capacity at place [1] --> e.g
    qm [1] or c_oo[1]

# Furthermore, if only one component is available --> the variables will set up at place [0]
    to ensure proper calculation.

if mfc2 is 0:
    print ('mfc2 = 0 --> component 1 will set to place [0]')

    mfc[0] = 1
    mfc[1] = 0
    qm[0] = qm1
    qm[1] = 0
    k [0] = Ka1
    k[1] = 0
    c_0[1] = 0
```

```python
    c_0[0] = c_01

elif mfc1 is 0:
    print ('mfc1 = 0 —> component 2 will set to place [0]')

    mfc[0] = 1
    mfc[1] = 0
    qm[0] = qm2
    qm[1] = 0
    c_0[0] = c_02
    c_0[1] = 0
    k[0] = Ka2
    k[1] = 0

elif qm1 > qm2:
    print ('setting component 1 to place [1]')

    qm[1] = qm1
    qm[0] = qm2
    k[1] = Ka1
    k[0] = Ka2
    c_0[1] = c_oo[0]
    c_0[0] = c_oo[1]

else:
    print ('setting component 2 to place [1]')

    qm[1] = qm2
    qm[0] = qm1
    k[1] = Ka2
    k[0] = Ka1
    c_0[1] = c_oo[1]
    c_0[0] = c_oo[0]

# co describes the x−axis of that component which is set to place [0]. Its important for
    calculation .

# for every co —> q and c1 will be computated

co = np.linspace(0,c_0[0],steps)

# xo are the start conditions

xo = np.array([0,0,0])

# for single component is delta = 0

delta = qm[0]/qm[1]

setting component 2 to place [1]


Definition of function; Solver; Plot
In [29]:

#def of function

def f2min(x,k,c_0,qm,co,delta,epsilon):
    f = np.zeros(3)
    q = x[0:2]
    c1 = x[2:3]

#implicit function —> extendend multicomponent qo
```

Appendix A. Python source code for the full competitve extendend Langmuir isotherm

```
    f[0] = q[0]*(1+k[1]*c1) + k[0]*c0*(q[0] + (1-delta)*k[1]*c1*q[0] - qm[0] - k[1]*c1*qm[0]
        + delta*k[1]*c1*qm[1])

#implicit function --> extendend multicomponent q1

    f[1] = q[1]*(1+k[0]*c0) + k[1]*c1*(q[1] + (1-delta)*k[0]*c0*q[1] - qm[1] - k[0]*c0*qm[1]
        + k[0]*c0*qm[0])

#implicit function --> theta extended =Vresin/Vsolution --> theta0 - theta1 = 0

    f[2] = (c_0[0]-c0)*q[1] - (c_0[1]-c1)*q[0] + epsilon*(c_0[0]*c1 - c_0[1]*c0 - q[1]*c0 + q
        [0]*c1)

    return f

#Solver

x_all=[]

for i in range(len(c0)):

    opt=optimize.root(f2min,x0,(k,c_0,qm,c0[i],delta,epsilon), method= 'hybr')

    x0=opt.x
    x_all.append(opt.x)
x_all = np.array(x_all)

#additional functions for plotting issues

theta[0] = x_all[:,0]/qm[0]    #fractional occupancy of component 1
theta[1] = x_all[:,1]/qm[1]    # fractional occupancy of component 2
summe = np.array([np.zeros(2),steps])
summe = (theta[0] + theta[1])
conorm = c0/c_0[0]
c1norm = x_all[:,2]/c_0[1]

#Plot 1: Normal Plot

fig = plt.figure()
plt.plot(x_all[:,2],x_all[:,1],'k--',label = names[2])
plt.plot(c0,x_all[:,0],'k-', label = names[1])
plt.legend(loc = 'best',fontsize = 12)
plt.xlabel(r'$c_i$ in supernatant $(\frac{mg}{mL})$', fontsize = 14)
plt.ylabel(r'$q_i$ $(\frac{mg}{mL})$', fontsize = 14)
#fig.suptitle('2-component adsorption isotherme')
plt.xlim (0,c_0[0])
plt.ylim(0,qm[1])

#plot 2: Fractional Occupancy vs. Normalized x-Axis of component 1

fig = plt.figure ()
plt.plot(conorm,theta[1],'k--', label=names[2])
plt.plot(conorm,theta[0],'k-',label = names[1])
plt.plot(conorm,summe,'k-.', label = 'Both components')
plt.xlim(0,1)
plt.ylim(0,1)
plt.xlabel(r'$(c_1 / c_1^0)$',fontsize = 14)
plt.ylabel(r'$\theta_i$ ', fontsize = 14) #theta = occupied / unoccupied sites
#plt.suptitle(r'Fractional occupancy against normalized £c_1£')
plt.legend(loc = 'best', fontsize = 12)

#plot 3: Fractional Occupancy vs. Normalized x-axis of Component 2
```

61

Appendix A. Python source code for the full competitve extendend Langmuir isotherm

```
fig = plt.figure ()
plt.plot(c1norm,theta[1],'k—',label = names[2])
plt.plot(c1norm,theta[0],'k—',label= names[1])
plt.plot(c1norm,summe,'k—.',label = 'Both components')
plt.legend(loc='best', fontsize = 12)
plt.xlim(0,1)
plt.ylim(0,1)
plt.xlabel(r'$(c_2 / c_2^0)$',fontsize = 14)
plt.ylabel(r'$\theta_i$ ',fontsize = 14)
#plt.suptitle(r'Fractional occupancy against normalized £c_2£')

#plot 4: Occupational relationship of both components

fig = plt.figure()
w= max(theta[0]) #help parameter for blotting the text and arrow
ww=r'$\theta_1=$'+"%.2f" %w   #help parameter for blotting the
#text and arrow
f= 1—w          #help parameter for blotting the text and arrow
for ind in [ind for ind, x in enumerate(theta[0]) if x == max(theta[0])]:
    print ind ,'Postion of Maximum in array'
z=theta[1][ind]
zz= r'$\theta_2=$'+"%.2f" %z
zw=(ww +Y zz)
www = w+0.1
plt.plot(theta[1],theta[0],'k—')
plt.ylim(0,1)
plt.xlim(0,1)
plt.xlabel(r'$\theta_2$',fontsize= 14)
plt.ylabel(r'$\theta_1$',fontsize= 14)
#plt.suptitle ('Occupancy rate of both components')
plt.annotate('', xy=(z,www),xytext=(1,www),xycoords='data',
arrowprops=dict(arrowstyle="<->",facecolor='black'))
bbox_props = dict(boxstyle="square",pad=0.3",fc="white",lw=1)
#aa=plt.text(0.015,0.945,zw, size=10, bbox=bbox_props) # written text over arrow
#bb=plt.text(f+0.05,w+0.05,'Displacement—Effect')
xticks = np.linspace(0,1.1,11,'')
yticks = np.linspace(0,1.1,11,'')
plt.xticks(xticks)
plt.yticks(yticks)
plt.grid()
```

Appendix B.

Recipe for PBS buffer

Table B.1 shows the recipe for a 10x phosphate saline buffer (PBS). The 1x PBS should exhibit a pH of 7.4 and a conductivity κ of around 14 $\frac{mS}{cm}$.

Table B.1.: Recipe for 10x PBS

reagent	concentration $[\frac{mol}{L}]$
Na_2HPO_4	0.100
KH_2PO_4	0.018
KCl	0.027
NaCl	1.37